PCCP

PAPER

View Article Online
View Journal | View Issue

Cite this: *Phys. Chem. Chem. Phys.*, 2025, **27**, 21563

General integrated rate law for complex self-assembly reactions reveals the mechanism of amyloid-beta coaggregation

Alexander J. Dear, *[abcd] Georg Meisl, [e] Emil Axell, [d] Xiaoting Yang,[d] Risto Cukalevski,[d] Thomas C. T. Michaels, [ab] Sara Linse [d] and L. Mahadevan *[c]

Analyzing kinetic experiments on protein aggregation using integrated rate laws has led to numerous advances in our understanding of the fundamental chemical mechanisms behind amyloidogenic disorders such as Alzheimer's and Parkinson's diseases. However, the description of biologically relevant processes may require rate equations that are too complex to solve using existing methods, hindering mechanistic insights into these processes. An example of significance is coaggregation in environments containing multiple amyloid-beta (Aβ) peptide alloforms, which may play a crucial role in the biochemistry of Alzheimer's disease but whose mechanism is still poorly understood. Here, we use the mathematics of Lie symmetry to derive a general integrated rate law valid for most plausible linear self-assembly reactions. We use it in conjunction with experimental data to determine the mechanism of coaggregation of the most physiologically abundant Aβ alloforms: Aβ42, Aβ40, Aβ38 and Aβ37 peptides. We find that Aβ42 fibril surfaces catalyze the formation of co-oligomers, which accelerate new Aβ40, Aβ38 and Aβ37 fibril formation whilst inhibiting secondary nucleation of new Aβ42 fibrils. The simplicity, accuracy and broad applicability of our general integrated rate law will enable kinetic analysis of more complex filamentous self-assembly reactions, both with and without coaggregation.

Received 3rd April 2025,
Accepted 11th September 2025

DOI: 10.1039/d5cp01288k

rsc.li/pccp

I. Introduction

The self-assembly of proteins and peptides into amyloid fibrils has been intensively studied in the past decades due to its key role in a multitude of increasingly prevalent and incurable human pathologies, such as type-II diabetes, Alzheimer's and Parkinson's diseases.[1,2] The kinetics of the self-assembly process have been found to be well-described by differential equations that, although relatively simple, do not normally possess exact analytic solutions. Instead, great success has been had in developing accurate approximate analytic solutions for several particularly important mechanisms of self-assembly.[3–9] These expressions have been widely fitted to experimental data in order to identify the constituent reaction steps and their associated rate constants for many different proteins under diverse conditions.[10] This has enabled fundamental discoveries about the chemical mechanisms behind the formation of both pathological and functional amyloid,[11,12] ranging from Amyloid-β and tau fibrils in Alzheimer's disease[6,9,13,14] to functional yeast prions in *S. cerevisiae*[15] and bacterial biofilms.[16] Such solutions are also used in the screening of candidate inhibitory drugs for the treatment of aggregation-related diseases.[17–19]

Now that many of the fundamental aggregation reactions in simple systems have been characterized, researchers have become increasingly interested in aggregation in complex systems. This requires less idealized and more realistic representations of the self-assembly process, described by more complex kinetic equations. In particular, interactions between different proteins or different forms of a protein during aggregation *in vivo* is expected to be the norm rather than the exception, given that biological environments tend to contain multiple self-assembly-prone species as well as other molecular factors in close proximity. For instance, post-translational modifications appear to play an important role during *in vivo* aggregation of tau,[20] but lead to a non-uniform monomer pool, and the coaggregation of lipids and protein likely plays an

[a] *Department of Biology, Institute of Biochemistry, ETH Zurich, Otto Stern Weg 3, 8093 Zurich, Switzerland. E-mail: alexander.dear@bc.biol.ethz.ch*
[b] *Bringing Materials to Life Initiative, ETH Zurich, Switzerland*
[c] *School of Engineering and Applied Sciences, Departments of Physics and of Organismic and Evolutionary Biology, Harvard University, Harvard, MA, USA. E-mail: lmahadev@g.harvard.harvard.edu*
[d] *Department of Biochemistry and Structural Biology, Lund University, 221 00 Lund, Sweden*
[e] *Yusuf Hamied, Department of Chemistry, University of Cambridge, Lensfield Road, Cambridge CB2 1EW, UK*

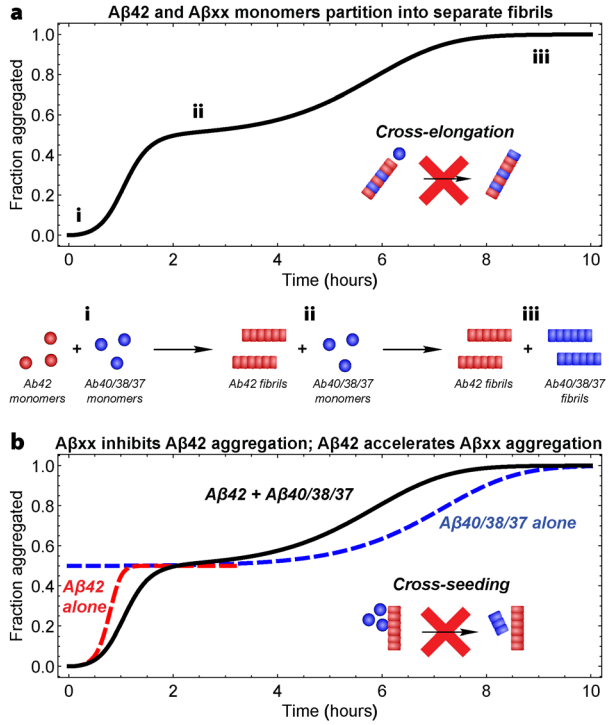

Fig. 1 Previously established mechanistic features of Aβ42 coaggregation with Aβ40/38/37 (Aβ*xx*), illustrated using typical kinetic curves for these reactions. (a) Aβ42 and Aβ*xx* coaggregation at pH 7.4 shows separate sigmoidal increases in fibril mass, with the first corresponding to pure Aβ42 fibril formation, and the second to pure Aβ*xx* fibril formation. Thus, no significant cross-elongation occurs. Representative kinetic curves (black) are generated from the later-determined integrated rate laws for Aβ alloform coaggregation (eqn (22)) using typical parameter values (see Table 1). (b) Monomeric Aβ*xx* has a clear inhibitory effect on Aβ42 fibril formation, whereas monomeric Aβ42 accelerates Aβ*xx* fibril formation. (Addition of pure Aβ42 fibrils to monomeric Aβ*xx* was found in ref. 30 and 31 not to accelerate or "cross-seed" nucleation of new Aβ*xx* fibrils.) The detailed mechanism of these inhibitory and accelerating effects was heretofore unknown and is a key focus of the present study. The red and blue curves are generated from published analytical solutions for Aβ40 and Aβ42 aggregation in isolation,[9] using the same parameter values as in *a* (see Table 1).

important role in α-synuclein aggregation.[21] Another particularly notable example is the large number of different length-variants (alloforms) and post-translationally modified variants of the Alzheimer's disease-associated Aβ peptide[22,23] that appear to be involved in aggregate formation during the disease. Several of these variants occur *in vivo* at non-negligible concentrations, and have been shown or proposed to have differing effects on both the aggregation rate and the progression of the disease.[22–29] A complete understanding of Alzheimer's disease will likely require a full understanding of the ways in which these proteins interact during aggregation into fibrils.

Some such coaggregation reactions have already been studied experimentally *in vitro*.[26,30–35] However, it was not possible at the time to derive analytical solutions to their rate equations, limiting the kinetic analysis that could be performed. The present study focusses on an example of particular biological significance: the coaggregation of the key Aβ alloforms Aβ40, Aβ37 or Aβ38 (hereafter referred to collectively as Aβ*xx*) with Aβ42. In recent studies[30,31] this has been monitored over time by Thioflavin T (ThT), a dye that fluoresces when it binds to amyloid fibrils, under physiologically relevant conditions (in 20 mM sodium phosphate and 0.2 mM EDTA at pH 7.4, without agitation). The resultant kinetic curves describing the transformation of monomeric to fibrillar protein feature two separate sigmoidal transitions (Fig. 1a).

Even in the absence of analytical solutions and their global fitting to kinetic data, a partial determination of the mechanism of coaggregation nonetheless proved possible in ref. 31 and 30. Using various biophysical techniques, the first transition was established to correspond to the formation of fibrillar Aβ42, and the second to the formation of fibrils consisting exclusively of Aβ*xx*.[30,31] This ruled out any significant cross-elongation reaction steps. Since the second sigmoid occurs much earlier than that observed for the corresponding shorter peptide in isolation, it was deduced that aggregation of new Aβ*xx* fibrils must nonetheless be accelerated by monomeric Aβ42, aggregated Aβ42, or the two together. The possibility that aggregated Aβ42 alone could cause this acceleration was ruled out directly by use of "cross-seeding" experiments. In these, pure pre-formed Aβ42 fibril seeds were added to pure Aβ*xx* monomers, which failed to significantly accelerate aggregation of the latter.[30,31] Since cross-elongation was ruled out, it was further deduced that "co-nucleation" reactions involving both Aβ42 and Aβ*xx* monomers cause the acceleration. It was also found that monomeric Aβ*xx* always inhibits the aggregation of Aβ42 (Fig. 1b). However, without the ability to solve analytically the rate equations describing different candidate reaction networks, it was not possible at the time to correctly identify or confirm the mechanisms of co-nucleation and cross-inhibition of these peptides.

This study makes 3 distinct scientific contributions. First, the Results section is devoted to the discovery of the molecular mechanisms of coaggregation of Aβ42 and Aβ*xx* alloforms. We derive the rate equations governing the various plausible candidate mechanisms, and present their solutions as calculated in the Methods. We next globally fit these solutions to both new and published experimental data on Aβ42 and Aβ*xx* coaggregation. We find that the central process driving coaggregation interactions is the catalytic formation of co-oligomers at the surface of Aβ42 fibrils. This both inhibits Aβ42 fibril formation and promotes Aβ*xx* fibril formation. For readers less focussed on the strategies we develop to solve rate equations, both the Methods and the SI can be skipped, without impairing understanding of the Results.

Second, the Methods section describes a formula giving the general solution for the kinetics of a very broad class of protein aggregation reactions, that includes many coaggregation reactions. We present a non-technical overview of how this general solution originates from the symmetry properties of the rate equations, and explain the conditions for its applicability. We then show that Aβ42–Aβ*xx* coaggregation satisfies these conditions, and demonstrate how the general solution formula can

be applied in practice by using it to solve the corresponding rate equations. We also briefly explain in the Methods (and at greater length in the SI) why the standard technique for deriving analytical solutions for simpler protein aggregation rate equations, fixed-point theory,[3–6] is unsuitable for most coaggregation reactions.

Third, the SI is focused on the development of a mathematical method based on Lie symmetries for solving differential equations of the kind governing protein aggregation kinetics. This method is then used to derive the general solution formula presented in the Methods. These findings constitute the detailed mathematical justification for the contents of the main text. They are nonetheless relegated to the SI because they are too technical to be accessible to a wide audience: although powerful and elegant, Lie theoretic techniques for differential equations are not widely known. In the Discussion we explore the implications both of our findings about Aβ coaggregation and of our mathematical method, their limitations, and prospects for future research.

II. Results

A. Rate laws for Aβ alloform coaggregation

We begin our analysis by building explicit kinetic models of Aβ42 aggregation in which the Aβ*xx* monomer inhibits one of the reaction steps. In keeping with convention for the field of amyloid kinetics, we use the letters m and M to denote the concentrations of free monomer and of monomeric subunits within fibrils, respectively. In a minor departure from convention in homomolecular kinetic models, we use P to refer to the concentration of fibril ends rather than fibril numbers. We do so since in principle a co-nucleation event could produce a fibril with an Aβ42 residue at one end and an Aβ*xx* residue at the other. This modifies the expressions for the various homomolecular rates by a factor of 2, as will be seen. To these letters we add the subscripts a and b to signify concentrations of species consisting of Aβ42 and Aβ*xx*, respectively. For example, m_a is the concentration of free monomeric Aβ42. In keeping with convention for amyloid kinetics we will use k_n, k_2 and k_+ for rate constants of primary and secondary nucleation and of elongation, respectively, and n_c and n_2 for the reaction orders of primary and secondary nucleation. To these we append brackets (a) and (b) to signify rate constants and reaction orders for homomolecular Aβ42 and for Aβ*xx* aggregation, respectively.

Aβ*xx* is almost entirely unaggregated during aggregation of Aβ42 in our coaggregation experiments (Fig. 1). Therefore, in this situation, none of the reaction steps responsible for Aβ42 fibril formation depend on P_b or M_b. Moreover, m_b is well-approximated as constant at its initial value $m_{\mathrm{tot},b}$ when modelling the aggregation of Aβ42 monomer into fibrils. So, the rates of the reaction steps responsible for Aβ42 fibril formation have time-dependence only *via* the variables m_a, M_a and P_a. Consequently, the first sigmoid, corresponding to Aβ42 aggregation, can be described by kinetic equations of the form:

$$\frac{\mathrm{d}P_a}{\mathrm{d}t} = \alpha_{1,a}(m_a) + \alpha_{2,a}(m_a)M_a, \tag{1a}$$

$$\frac{\mathrm{d}M_a}{\mathrm{d}t} = \alpha_{e,a}(m_a)P_a, \quad M_a + m_a = m_{\mathrm{tot},a}, \tag{1b}$$

where $\alpha_{1,a}$, $\alpha_{e,a}P_a$ and $\alpha_{2,a}M_a$ are the rates of primary nucleation, elongation and secondary nucleation respectively. The as-yet unknown functions $\alpha_{1,a}$, $\alpha_{e,a}$ and $\alpha_{2,a}$ express the dependence of these rates on the time-dependent variable m_a. In principle, $\alpha_{e,a}$ could be defined to also account for fibril depolymerization. However, we will neglect this possibility for simplicity, because the experiments analyzed in this study, as with almost all kinetic experiments on Aβ alloforms, use initial monomer concentrations far above the solubility limit. (For instance, under the conditions of this study this limit is <100 nM for Aβ42[36] and ~ 300 nM for Aβ40.[37]) Thus, these aggregation reactions are effectively irreversible, with depolymerization rates negligible in front of elongation rates. Consequently, depolymerization can be ignored without affecting modelling accuracy.[4]

Since the first sigmoidal transition is never accelerated by Aβ*xx*, any co-nucleation step must produce new Aβ42 fibrils much slower than ordinary Aβ42 primary nucleation. Thus, we may neglect co-nucleation in our models of Aβ42 aggregation. The dependence of the rates of each individual reaction step on $m_{\mathrm{tot},b}$ therefore purely reflects its inhibitory effects. Since the concentration of fibril ends and primary and secondary nucleation sites is typically low, monomer binding to them should be at partial or pre-equilibrium.[9] So, the inhibitory effects of Aβ*xx* monomer on Aβ42 primary nucleation and elongation can be modelled using the perturbed rate laws of ref. 18 and 38:

$$\alpha_{1,a}(m_a) = \frac{2k_n(a)m_a^{n_c(a)}}{1 + m_{\mathrm{tot},b}/K_{\mathrm{P}}(ba)}, \tag{2a}$$

$$\alpha_{e,a}(m_a)P_a = \frac{k_+(a)m_a}{1 + m_{\mathrm{tot},b}/K_{\mathrm{E}}(ba)}P_a, \tag{2b}$$

where $K_{\mathrm{P}}(ba)$ and $K_{\mathrm{E}}(ba)$ are equilibrium constants for dissociation of Aβ*xx* monomer from Aβ42 fibril ends and from Aβ42 primary nucleation sites, respectively.

Modelling inhibition of secondary nucleation is more complicated, because Aβ42 secondary nucleation is at least partly saturated under the reaction conditions (meaning that monomeric protein binds faster to the fibril surface than surface-bound monomer can convert to new fibrils[6]). The rate of inhibited secondary nucleation is found (see Appendix A) to be:

$$\alpha_{2,a}(m_a) = \frac{2k_2(a)m_a(t)^{n_2(a)}}{1 + (m_a(t)/K_{\mathrm{S}}(a))^{n_2(a)} + (m_a(t)/K_{\mathrm{S}}(ba))^{n_2(aa)}(m_b(0)/K_{\mathrm{S}}(ba))^{n_2(ab)}}, \tag{3}$$

where $K_{\mathrm{S}}(a)^{n_2(a)}$ is the dissociation constant for a cluster of $n_2(a)$ Aβ42 monomers from an Aβ42 fibril surface, and $K_{\mathrm{S}}(ba)^{n_2(aa)+n_2(ab)}$ the dissociation constant for a cluster of $n_2(aa)$ Aβ42 monomers and $n_2(ab)$ Aβ*xx* monomers from an Aβ42 fibril surface.

Since Aβ*xx* fibrils form in significant quantities only long after Aβ42 monomers, any interactions between the two can be neglected. (In any case, there is evidence that such interactions, if they exist, are weak[30]) So, it is reasonable to model the aggregation of Aβ*xx* monomers into fibrils as follows:

$$\frac{dP_b}{dt} = \alpha_{1,b}(m_a, m_b) + \alpha_{2,b}(m_b)M_b \tag{4a}$$

$$\frac{dM_b}{dt} = \alpha_{e,b}(m_b)P_b, \tag{4b}$$

$$\alpha_{1,b}(m_a, m_b) = \alpha_{1,bb}(m_b) + \alpha_{1,ba}(m_a, m_b) + \alpha_{2,ba}(m_a, m_b)M_a, \tag{4c}$$

where $\alpha_{2,b}$ and $\alpha_{e,b}$ correspond to the known rate laws[6,31] for Aβ40 and Aβ38 elongation and secondary nucleation (modified by a factor of 2, as discussed above):

$$\alpha_{e,b}(m_b) = k_+(b)m_b \tag{5a}$$

$$\alpha_{2,b}(m_b) = \frac{2k_2(b)m_b^{n_2(b)}}{1 + (m_b/K_S(b))^{n_2(b)}}, \tag{5b}$$

The total Aβ*xx* primary nucleation rate $\alpha_{1,b}$ contains contributions from the rates of production of new Aβ*xx* fibril ends *via* primary co-nucleation and secondary co-nucleation on Aβ42 fibrils, $\alpha_{1,ba}$ and $\alpha_{2,ba}M_a$ respectively, as well as the rate of normal Aβ*xx* primary nucleation $\alpha_{1,bb}$. These rates are:

$$\alpha_{1,bb}(m_b) = 2k_n(b)m_b^{n_c(b)} \tag{6a}$$

$$\alpha_{1,ba}(m_a, m_b) = 2k_n(ba)m_a^{n_c(ba)}m_b^{n_c(bb)} \tag{6b}$$

$$\alpha_{2,ba}(m_a, m_b)M_a = 2k_2(ba)m_a^{n_2(ba)}m_b^{n_2(bb)}M_a. \tag{6c}$$

Note that, from the point of view of Aβ*xx*, the Aβ42 fibrils are just another heterogeneous nucleation surface, whose abundance is not increased directly by the formation of more Aβ*xx* fibrils. It has been demonstrated that primary nucleation is usually overwhelmingly heterogeneous, occurring at nucleation sites such as plate surfaces or the air–water interface rather than in free solution.[9,39–44] This is why secondary co-nucleation on Aβ42 fibrils enters the primary nucleation term for Aβ*xx*, rather than contributing to Aβ*xx* secondary nucleation.

B. Aβ40 and Aβ38 monomers bind to Aβ42 fibril surfaces, inhibiting secondary nucleation

In Methods Section V A we present a general class of rate equations, eqn (11), governing many protein reactions. In Methods Sections V B–V D we outline how we solve those equations, concluding with a general solution formula, eqn (16), alongside conditions for its applicability. In Methods Section V E1 we confirm that eqn (1)–(3) fall into the class of eqn (11), and demonstrate that they satisfy the conditions for applicability of eqn (16). This is finally used to calculate the explicit solution eqn (22). In the absence of seed, this simplifies to:

$$\frac{M_a(t)}{m_a(0)} = 1 - \left[1 + \frac{\varepsilon_a}{c_a}(e^{\kappa_a t} + e^{-\kappa_a t} - 2)\right]^{-c_a} \tag{7a}$$

$$c_a = \frac{3}{2n_2'(a) + 1}, \quad \kappa_a = \sqrt{\alpha_{e,a}(m_{\mathrm{tot},a})\alpha_{2,a}(m_{\mathrm{tot},a})} \tag{7b}$$

$$\varepsilon_a = \frac{\alpha_{1,a}(m_{\mathrm{tot},a})}{2m_{\mathrm{tot},a}\alpha_{2,a}(m_{\mathrm{tot},a})}, \tag{7c}$$

where $n_2'(a)$ interpolates between $n_2(a)$ and 0 depending on the degrees of saturation and inhibition, and is given by eqn (21). This solution corresponds closely to the numerically integrated rate eqn (7a). As $K_S(a)/m_{\mathrm{tot},a}$ and $K_S(ba)/m_{\mathrm{tot},b} \to \infty$ (*i.e.* when initial monomer concentration is far below the saturation concentration), single-step kinetics are recovered as required.

It is known that, under the reaction conditions employed in the studies whose Aβ alloform coaggregation data we are revisiting ([30,31]), secondary nucleation of Aβ42 is saturated at all but the lowest monomer concentrations, with a dissociation constant of 1.1 μM,[45] and $n_c = n_2 = 2$. We confirm these parameter values by fitting in SI Section S7 a standard saturating secondary nucleation model[6] to homogeneous Aβ42 aggregation experiments conducted in the same studies.

Using these values, we then test eqn (7) against data for Aβ42–Aβ40 coaggregation and that for Aβ42–Aβ38 coaggregation, both truncated after the first sigmoid. Allowing inhibition only of primary nucleation by setting $K_E(ba)^{-1} = K_S(ba)^{-1} = 0$ and fitting $K_P(ba)$ (Fig. 2a), or only of elongation by setting $K_P(ba)^{-1} = K_S(ba)^{-1} = 0$ and fitting $K_E(ba)$ (Fig. 2b), yields misfits. However, allowing inhibition only of secondary nucleation by setting $K_P(ba)^{-1} = K_E(ba)^{-1} = 0$ and fitting $K_S(ba)$ yields good fits in both systems (Fig. 2c), providing strong evidence that at the concentrations investigated here Aβ*xx* inhibits predominantly Aβ42 secondary nucleation.

The apparent specificity of the inhibitory effect of Aβ*xx* monomers to this step alone implies they achieve this effect by binding to the surface of Aβ42 fibrils. This follows since the other possible binding targets participating in secondary nucleation, oligomers and monomers, also participate in other reaction steps. In Appendix B, we use global fitting to a larger Aβ42–Aβ40 coaggregation dataset (including previously unpublished data) to determine the most likely mechanism for this inhibition. We find this to be the co-operative binding of Aβ42 and Aβ*xx* monomers to nucleation sites on Aβ42 fibrils (*i.e.* $n_2(aa) = n_2(ab) = 1$), which then forms co-oligomers that do not readily convert to new Aβ42 fibrils. Inhibition instead by non-*co*-operative binding of individual Aβ*xx* monomers to nucleation sites on Aβ42 fibrils is found to be less likely although not impossible. (Although its model gives worse fits, they are not poor enough to rule out this model altogether.) Note, the mechanism of inhibition was also investigated in ref. 31, but without a detailed kinetic model of the possible inhibition modes being available at the time, the fits and misfits were prepared simply by allowing the Aβ42 rate constants to take different values for different Aβ*xx* concentrations. This approach

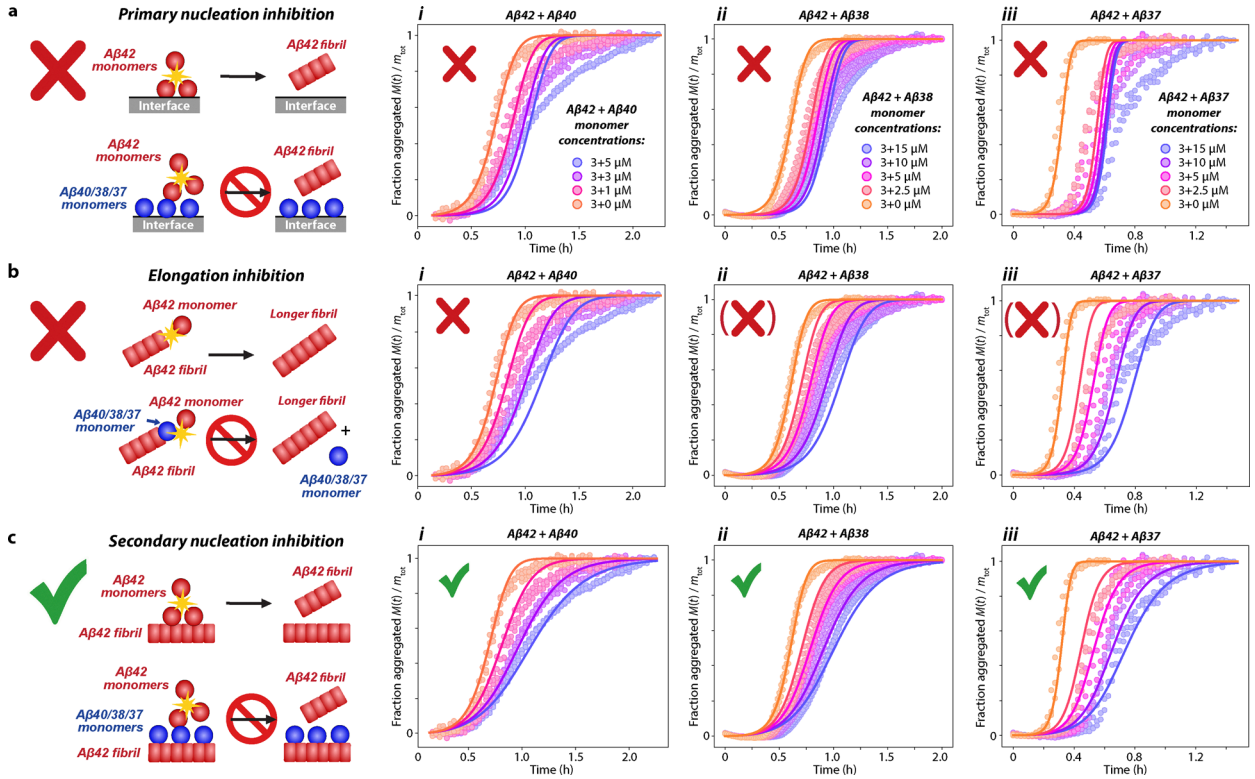

Fig. 2 Kinetic analysis of first sigmoid of coaggregation data reveals molecular mechanism of Aβ42 aggregation inhibition by Aβ*xx*. Monomeric Aβ42 (3 μM) was aggregated with various initial Aβ40 (i), Aβ38 (ii) or Aβ37 (iii) monomer concentrations. (a) Global misfits of model in which Aβ*xx* inhibits primary nucleation (eqn (7) with $K_E(ba)^{-1} = K_S(ba)^{-1} = 0$). Mean residual errors (MREs) are 7.9×10^{-3} (i), 4.9×10^{-3} (ii), 1.4×10^{-2} (iii). (b) Global misfits of model in which Aβ*xx* inhibits elongation (eqn (7) with $K_P(ba)^{-1} = K_S(ba)^{-1} = 0$). MREs are 4.9×10^{-3} (i), 3.7×10^{-3} (ii), 9.4×10^{-3} (iii). (c) Global fits of model in which Aβ*xx* inhibits secondary nucleation (eqn (7) with $K_E(ba)^{-1} = K_P(ba)^{-1} = 0$). MREs are 1.8×10^{-3} (i), 1.9×10^{-3} (ii), 5.2×10^{-3} (iii). Fitted parameter values are summarized in Tables S1–S3. Individually for each Aβ*xx* alloform, the improvement in fit quality from b to c is arguably insufficient to eliminate the elongation inhibition mechanism with high confidence. (Brackets around the misfit "X" symbol indicate when the MREs are slightly less than double those achieved with the model used in (c).) However, collectively they provide strong evidence in favour of secondary nucleation inhibition being the dominant cause of overall inhibition.

was consequently insufficiently precise to distinguish elongation inhibition from secondary nucleation inhibition.

It has been convincingly ruled out under the physiologically relevant reaction conditions used in this study[30,31] that Aβ42 fibrils alone can catalyze the aggregation of Aβ*xx* anywhere near as strongly as can monomeric Aβ42 under the physiologically relevant reaction conditions used in this study.[30,31] In other words, the formation of pure Aβ*xx* nuclei or oligomers is not strongly catalysed by Aβ42 fibril surfaces. Indeed, our fitting results in Appendix B further confirm this earlier finding, by ruling out that formation of such oligomers could drive the inhibition by Aβ*xx* of Aβ42 secondary nucleation. This is additionally supported by the results of (Fig. 2c), where $n_2(ab)$ is also fitted and found to be approximately 1 in all three coaggregation reactions.

C. Aβ42 accelerates Aβ40 aggregation predominantly by enabling secondary co-nucleation

When Aβ42 aggregation is complete before that of the other peptide, we may use the analytical solution eqn (7) for $m_a(t)$ and $M_a(t)$ in the rate laws for Aβ*xx* fibril formation, eqn (4) (or eqn (22) when Aβ42 fibril seeds are present). In Methods Section V E2 we confirm that under this condition eqn (4) is an example of the general class of rate equations eqn (11), and verify the applicability of the general solution formula eqn (16). This is then used to calculate the following solution (validated against numerical integration in Fig. 7):

$$\frac{M_b(t)}{m_b(0)} = 1 - \left[1 + \frac{\tilde{\varepsilon}_b}{c_b}\left(e^{\kappa_b t} + e^{-\kappa_b t} - 2\right)\right]^{-c_b} \tag{8a}$$

$$c_b = \frac{3}{2n_2'(b) + 1}, \quad \kappa_b = \sqrt{\alpha_{e,b}(m_{\mathrm{tot},b})\alpha_{2,b}(m_{\mathrm{tot},b})} \tag{8b}$$

$$\tilde{\varepsilon}_b = \frac{\alpha_{1,bb}(m_{\mathrm{tot},b}) + f_1\alpha_{1,ba}(m_{\mathrm{tot},a}, m_{\mathrm{tot},b}) + f_2 m_{\mathrm{tot},a}\alpha_{2,ba}(m_{\mathrm{tot},a}, m_{\mathrm{tot},b})}{2m_{\mathrm{tot},b}\alpha_{2,b}(m_{\mathrm{tot},b})}, \tag{8c}$$

where $n_2'(b)$ is given by eqn (27) and interpolates between $n_2(b)$ and 0 depending on the extent of saturation of secondary nucleation, similarly to $n_2'(a)$. $f_1\alpha_{1,ba}$ and $f_2 m_{\mathrm{tot},a}\alpha_{2,ba}$ are constants that express the contributions from primary and secondary co-nucleation to the effective total rate of primary nucleation of Aβ*xx* fibrils. Co-nucleation enters nowhere else in the equation. The constants f_1 and f_2 are positive but <1

(see below, and Section V E2), reflecting that co-nucleation is present during only part of the lag phase for Aβ*xx* fibril formation, until Aβ42 monomers are depleted. Therefore, the only effect of co-nucleation is to shift the second sigmoid in the kinetic curves (corresponding to Aβ*xx* fibril formation) to earlier times, as observed experimentally in ref. 30 and 31.

The dependence of the effective co-nucleation rate $f_1\alpha_{1,ba} + f_2 m_{\mathrm{tot},a}\alpha_{2,ba}$ on the Aβ42 seed concentrations $M_a(0)$ and $P_a(0)$ gives us a way to distinguish primary and secondary co-nucleation experimentally. f_1 and f_2 depend on seed concentrations as follows:

$$f_1 = 1 - \left(2\varepsilon_a + \frac{M_a(0)}{m_{\mathrm{tot},a}} + \frac{2k_+(a)}{\kappa_a}P_a(0)\right)^{\frac{\kappa_b}{\kappa_a}}\bar{f}_1, \tag{9a}$$

$$f_2 = \left(2\varepsilon_a + \frac{M_a(0)}{m_{\mathrm{tot},a}} + \frac{2k_+(a)}{\kappa_a}P_a(0)\right)^{\frac{\kappa_b}{\kappa_a}}\bar{f}_2. \tag{9b}$$

$\bar{f}_1, \bar{f}_2 > 0$ are constants depending on the parameters entering the Aβ42 aggregation rate equations, whose precise forms are given in eqn (24).

Crucially, as seed concentrations $M_a(0)$ and $P_a(0)$ are raised, f_2 increases but f_1 decreases. So if Aβ42 influences Aβ*xx* kinetics *via* primary co-nucleation ($\alpha_{2,ba} = 0$), increasing Aβ42 seed concentrations should *decrease* co-nucleation overall and delay the second sigmoid to later times. Conversely, if Aβ42 influences Aβ*xx* kinetics *via* secondary co-nucleation ($\alpha_{1,ba} \ll m_{\mathrm{tot},a}\alpha_{2,ba}$), increasing Aβ42 seed concentrations should *accelerate* Aβ*xx* aggregation and shift the second sigmoid to earlier times. An intuitive justification is as follows. The rate of secondary co-nucleation is proportional to Aβ42 fibril concentration so is promoted by Aβ42 seed addition, at least at low seed concentrations. However, the rate of primary co-nucleation is not directly dependent on Aβ42 fibril concentration. Instead, adding Aβ42 seed indirectly reduces the primary co-nucleation rate by accelerating Aβ42 aggregation, reducing the amount of time during which both monomeric Aβ42 and Aβ*xx* are simultaneously present.

While in previous work we correctly identified the formation of co-oligomers as the key step accelerating Aβ*xx* aggregation,[30] the proposal that this co-nucleation of Aβ42 and Aβ*xx* is primary does not hold in our current, more complete analysis. The key observation that led to this proposal in ref. 30 was an experiment monitoring the formation of Aβ40 fibrils during aggregation of a 1 : 1 mixture of Aβ42 and Aβ40 monomers with the addition of different concentrations of Aβ42 fibril seeds (Fig. 7A of ref. 30). We concluded then that there was no significant dose-dependent effect on the rate of Aβ40 with varying Aβ42 seed. However, in light of the mechanistic conclusions obtained above by application of our analytical solutions, we have revisited these data. Applying more stringent data processing to remove noise (see Methods Section V G), a steady increase in the Aβ40 aggregation rate with Aβ42 seed concentration becomes apparent (Fig. 3i and ii), as would be expected for secondary not primary co-nucleation.

To confirm that secondary co-nucleation dominates over primary co-nucleation, we first fit eqn (7) to the data truncated after the first sigmoid to determine Aβ42 aggregation rate constants for this particular experiment. The overall kinetic curves are described by:

$$M(t) = \frac{M_a(t) + M_b(t)}{m_{\mathrm{tot},a} + m_{\mathrm{tot},b}}, \tag{10}$$

where $M_a(t)$ and $M_b(t)$ are given by eqn (7) and (8), respectively. Using these parameters we then test eqn (10) with either primary or secondary co-nucleation rate constants set to zero against the full kinetic dataset, yielding fits or misfits respectively (Fig. 3a and b). To further confirm this finding we perform a new seeded coaggregation experiment using different monomer concentrations; again, fits and misfits reveal that only secondary co-nucleation is consistent with the new data (Fig. 3iii). Fitted parameters are given in Tables S4 and S5. The data for the highest seed concentration used in ref. 30 ($M_a(0)/m_{\mathrm{tot,a}} = 0.25$) is excluded from our new analysis in Fig. 3i and ii, because at this concentration the assumption of low seed concentration used to derive the analytical model is violated. The half-time of the second sigmoid of the kinetic curve in this excluded dataset is actually increased relative to the next-highest seed concentration; this is a key reason why no effect of Aβ42 seeds on coaggregation was recognized in previous analysis.[30] Qualitatively, however, this remains consistent with a secondary co-nucleation mechanism. It can be rationalized as being due to the rapid depletion of monomeric Aβ42 at such high seed concentrations outweighing the increased availability of Aβ42 fibril surface. It is also plausible that at such high Aβ42 fibril concentrations, a significant proportion of monomeric Aβ40 becomes bound to the Aβ42 fibril surfaces without nucleating,[46] further slowing the kinetics of Aβ40 fibril formation.

D. Co-oligomer formation on Aβ42 fibril surfaces underpins both coaggregation and cross-inhibition phenomena

The formation of co-oligomers of Aβ42 and Aβ*xx* *via* primary nucleation has been observed experimentally.[47,48] Our findings confirm the proposal made in ref. 30 and 31 that such co-oligomers are responsible for the acceleration of Aβ*xx* fibril formation in these coaggregation reactions. However, these studies assumed that these co-oligomers are formed directly through primary nucleation. In contrast, we find that the formation of these co-oligomers is strongly catalyzed by Aβ42 fibril surfaces. Consequently only a small minority are formed directly through primary nucleation, and these ''primary co-oligomers'' therefore cannot significantly drive the acceleration of Aβ*xx* fibril formation, which is instead driven by the ''secondary co-oligomers''.

The same proposed mechanism can simultaneously explain our findings in this study that Aβ42 secondary nucleation is inhibited by Aβ*xx* monomers. The formation of these secondary co-oligomers requires binding of Aβ*xx* monomers to the secondary nucleation catalytic sites on Aβ42 fibrils. The occupation by these co-oligomers and/or Aβ*xx* monomers of the catalytic sites then prevents the formation of pure Aβ42

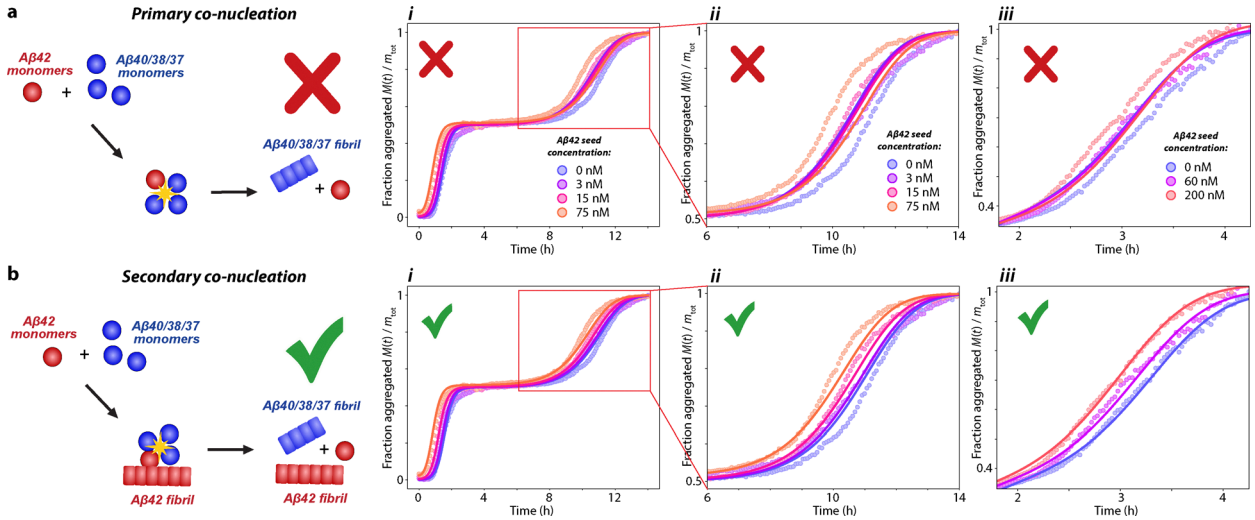

Fig. 3 Kinetic analysis of second sigmoid of seeded coaggregation data reveals molecular mechanism of Aβ*xx* aggregation acceleration by Aβ42. (i) and (ii) Kinetic data from Fig. 7 of ref. 30, showing coaggregation of 1.5 μM each of monomeric Aβ42 and Aβ40 with several concentrations of preformed Aβ42 fibril seeds, was additionally processed to suppress noise (see Methods V G). This reveals a clear trend of decreasing second sigmoid half-time with increasing Aβ42 seed concentration. (iii) We confirm this trend by performing a similar experiment but using different monomer concentrations (2 μM Aβ42 + 4 μM Aβ40; seed concentrations in legend). Only the second sigmoid is shown here; full timecourse is shown in Fig. S4. (a) Global misfits to full kinetic curves for Aβ42–Aβ40 coaggregation using model in which only primary co-nucleation occurs (eqn (10) with $k_2(ab) = 0$). (b) Global fits to full dataset for Aβ42–Aβ40 coaggregation using model in which only secondary co-nucleation occurs (eqn (10) with $k_n(ab) = 0$; fitted parameter values are summarized in Tables S4 and S5).

oligomers there. The inhibitory effect on Aβ42 secondary nucleation comes from the propensity of these co-oligomers to convert into fibrils of Aβ42 morphology being much lower than for pure Aβ42 oligomers. Additionally, any Aβ*xx* monomers occupying the catalytic sites alone can clearly not convert into Aβ42 fibrils. The promotion of heterogeneous nucleation of Aβ*xx* fibrils comes from these small heteromolecular intermediates having either a greater formation rate or a greater propensity to convert to fibrils of Aβ*xx* morphology than do pure Aβ*xx* nucleation intermediates *via* primary nucleation.

From the available data, it cannot be conclusively determined whether the inhibition of Aβ42 secondary nucleation is driven by the catalytic sites being occupied more by co-oligomers or by Aβ*xx* monomers under these conditions. However, we judge the former to be more likely since it is supported by the evidence presented in Appendix B that Aβ*xx* monomers bind co-operatively with Aβ42 monomers to Aβ42 fibrils. This unified mechanism is summarized schematically in Fig. 4. The involvement of Aβ42 monomers in binding of Aβ*xx* to these catalytic sites is additionally consistent with the known sequence specificity of amyloid-β secondary nucleation,[49] and with the findings in ref. 30 and 31 and in Results Section II B that pure Aβ*xx* nuclei or oligomers cannot easily form on Aβ42 fibril surfaces.

To validate our mechanistic model as conclusively as possible, we finally fit eqn (10) to unseeded full-timecourse kinetic data featuring multiple different monomeric protein concentrations for both Aβ42 + Aβ40 coaggregation (data from ref. 30) and Aβ42 + Aβ38 coaggregation (data from ref. 31). This yields good fits to both the full Aβ42–Aβ40 dataset (Fig. 5a) and the full Aβ42–Aβ38 dataset (Fig. 5b). The fitted rates of co-nucleation confirm the predictions of ref. 30 and 31 that co-nucleation produces new Aβ*xx* fibrils much faster than self-nucleation of Aβ*xx*. (Reproducibility of the second sigmoid of Aβ42–Aβ37 coaggregation data is too low to permit global fitting.[31])

III. Discussion

An implication of our finding that Aβ42 fibrils promote Aβ40 aggregation is that Aβ42 fibril formation may be upstream in the *in vivo* formation of fibrils consisting of the much more common Aβ40. Should this apply to the interaction of Aβ42 with other peptides, then the relatively rapid Aβ42 fibril formation may be upstream in the formation of a number of other kinds of fibrils. As well as providing a possible mechanistic link between different amyloid diseases, it raises interesting questions as whether the morphology of the fibrils of other peptides could under certain circumstances be influenced by the morphology of Aβ42 fibrils. We have found no evidence of changes in elongation and secondary nucleation rate constants for Aβ*xx* fibrils formed in the presence of Aβ42. Consequently, a changed morphology for Aβ*xx* fibrils seems unlikely under the conditions studied here. However, if the formation of fibrils of other kinds of peptides can be promoted by Aβ42 fibrils in the same way, then this possibility should be considered.

It is long-established that pure Aβ42 or Aβ40 nucleation also occurs predominantly on fibril surfaces,[6,13] *via* the surface-catalyzed formation of metastable oligomeric intermediates.[50] Our discovery in this study that co-nucleation of heteromolecular Aβ42–Aβ*xx* intermediates occurs predominantly on (Aβ42)

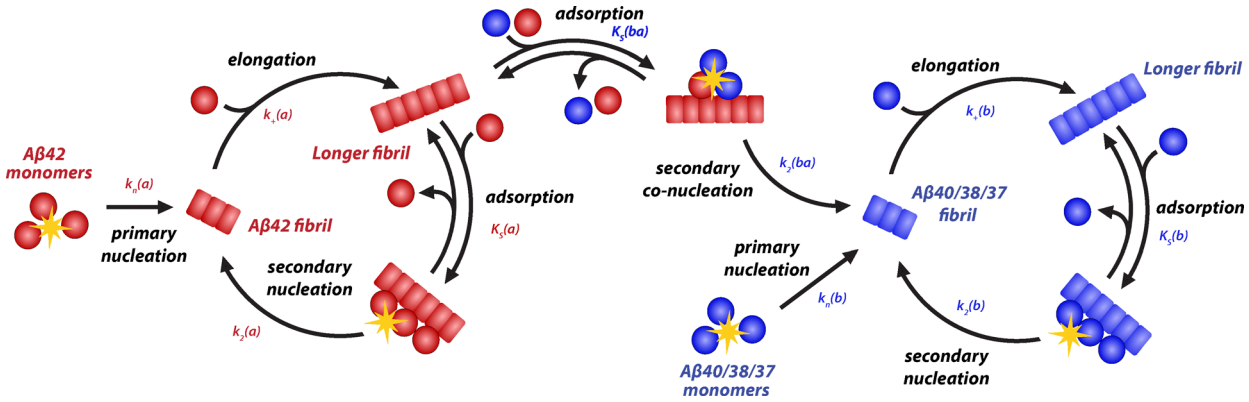

Fig. 4 Schematic of unified coaggregation model including all key states and reaction steps. Aβ*xx* monomers inhibit pure Aβ42 secondary nucleation by competing with Aβ42 monomers for catalytic sites on Aβ42 fibrils. Co-oligomers therefore form at these sites instead of pure Aβ42 clusters. The co-oligomers undergo structural rearrangement into new growth-competent Aβ*xx* fibrils, faster than they can form *via* primary nucleation. Any conversion of these co-oligomers into growth-competent Aβ42 fibrils is slow enough that Aβ42 secondary nucleation is still inhibited overall. Note, formation of larger heterogeneous on-pathway nucleation intermediates such as protofibrils, rather than co-oligomers, would be equally consistent with the experimental findings, although co-oligomers are known to form in these reactions.[47]

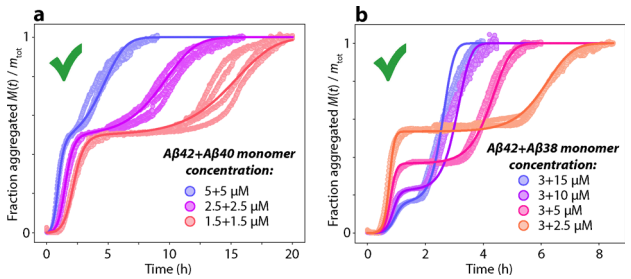

Fig. 5 Unified coaggregation model can successfully describe full kinetic curves for unseeded aggregation reactions using multiple initial concentrations of monomeric Aβ*xx*. (a) Global fit to full timecourse for Aβ42–Aβ40 coaggregation using unified model (eqn (10)); fitted parameter values are summarized in Table S6. (b) Global fit to full timecourse for Aβ42–Aβ38 coaggregation using unified model (eqn (10)); fitted parameter values are summarized in Table S2.

fibril surfaces rather than in solution should therefore perhaps not be surprising in hindsight. That such intermediates are formed predominantly by secondary nucleation rather than primary nucleation, in competition with pure Aβ42 intermediates simultaneously explains both the acceleration of Aβ*xx* nucleation by Aβ42 and the inhibition of Aβ42 secondary nucleation by Aβ*xx*. Occam's razor therefore lends further support to our mechanistic interpretation of the coaggregation and cross-inhibition effects over other potential mechanisms (such as primary co-nucleation with inhibition of elongation) that would generally rely on two distinct microscopic phenomena.

Our findings also provide a possible route to reconcile seemingly conflicting results in the literature regarding cross-seeding. In ref. 30 it was shown that Aβ42 fibrils alone cannot seed aggregation of Aβ40 monomer. Yet, numerous other studies have found at least a weak cross-seeding effect between these peptides.[33] Our results imply that even a small amount of Aβ42 monomer (or potentially some other Aβ variant) present as an impurity in such reactions could trigger cross-seeding. There are multiple ways such impurities could appear, including *e.g.*, disaggregation of a fraction of the Aβ42 seed fibrils due to storage at low temperature where their solubility is higher, or length and sequence variants inevitably present in synthetic Aβ42 batches. Although other explanations for cross-seeding differences exist, such as differences in reaction conditions, the unintended presence of monomeric peptide impurities should be considered as a possible candidate.

Despite the successes of our analysis, there remains some uncertainty in the precise mechanism of inhibition of Aβ42 secondary nucleation under the present experimental conditions. If we discount the tentative evidence presented in Appendix B, it remains plausible that Aβ*xx* monomers alone can also bind catalytic sites on Aβ42 fibrils, contributing to or even causing most of the inhibition. This possibility is supported by published experimental results showing Aβ42 fibrils being coated with pure Aβ40 monomers. For example, Aβ42 fibrils with added Aβ40 monomer are better dispersed and provide better contrast in cryo-transmission electron microscopy compared to pure Aβ42 fibrils.[51] Moreover, the results of surface plasmon resonance experiments show that Aβ40 monomers fail to elongate immobilized Aβ42 fibrils, yet a saturable binding curve is observed suggesting the binding of Aβ40 monomers to the sides of Aβ42 fibrils.[46] Although these results support the finding that Aβ*xx* monomers inhibit Aβ42 secondary nucleation, it also suggests that Aβ*xx* monomers can still bind Aβ42 fibrils in the absence of Aβ42 monomers, albeit potentially with lower affinity or specificity. On the other hand, only binding to the relatively rare catalytic sites for nucleation[52] is directly relevant for inhibition. This cannot be distinguished by such experiments from binding to non-catalytic regions of the fibril surface. Even if Aβ*xx* monomers on their own can bind such sites, this inhibition could be much weaker than that caused by co-oligomer formation. Although beyond the scope of the present paper, establishing a feasible experimental

approach to distinguish these closely related mechanisms could be a productive research direction for future studies.

Beyond Aβ42–Aβ*xx* coaggregation, our general solution formula is applicable to a broad range of possible protein aggregation reactions. This includes reactions with all three known secondary processes: secondary nucleation, fragmentation and branching. Indeed, the solution derived in ref. 8 that covers all such processes can be almost trivially derived using our formula (see SI Section S4B). It also includes reactions in which any or all of the reaction steps exhibit saturation: again, the universal solutions presented in ref. 9 for such reactions can be straightforwardly derived using our formula (see SI Section S5). In SI Section S4B we explain that this is because the derivation in ref. 9 unwittingly used a similar Lie symmetry transformation to that used to derive the general solution formula in the present study. In a follow-on study[53] citing the preprint version of the present study, we also use the general solution formula to derive an analytical solution for the kinetics of a protein aggregation reaction in which any or all species can be bound by an inhibitor. Another study[54] citing the preprint uses the method to derive solutions for the kinetics of protein aggregation with a source term, *e.g.* due to the generation of aggregation-prone monomer *in situ* from a precursor. Collectively, and including all possible permutations, these various solutions listed cover well over 100 possible protein aggregation reaction mechanisms. Although the derivation of the general solution formula is challenging, being rooted in a little-known sub-field of the specialized field of Lie symmetry analysis of differential equations, its practical application is straightforward. The remarkably simple form of the solutions it produces permits easy analysis of the kinetics. Alongside the lack of alternatives for solving more complicated protein aggregation rate equations, we expect these factors will result in widespread adoption of this method, through availability of updated models on the web-based fitting platform AmyloFit.[10] It should find immediate application in the analysis of kinetic experiments in other more complex biochemical systems involving protein aggregation in model mixtures, *in vivo* or in body fluids, and in the search for drugs that can inhibit critical reaction steps in this process.

The general solution formula, and the mathematical method underlying it outlined in the SI, nonetheless have some limitations, discussed in detail in the Methods. Some important examples of protein aggregation reactions to which the general solution formula is consequently inapplicable include highly seeded reactions (*i.e.* with large initial fibril concentrations), and reactions with very slow secondary processes. Both of these cases require a further generalization of the method, that we perform in a follow-on study.[53] Another limitation of the general solution formula that is yet to be addressed is that it is inapplicable to rate equations that explicitly track concentrations of nucleation intermediates such as oligomers. This includes the rate equations presented in ref. 50 and 55 and other studies. Since the majority of protein aggregation reactions are believed to involve such intermediates,[55] using our Lie symmetry method to develop a new general solution formula for such classes of rate equation would be a worthwhile subject for a future study.

VI. Conclusions

In summary, we have introduced a general mathematical approach to solving nonlinear rate equations of a kind frequently encountered in self-assembly reactions. We have applied it to derive integrated rate laws for the coaggregation of Aβ42 with other amyloidogenic peptides, which is a key event in Alzheimer's disease. By globally fitting these rate laws to both new and published experimental data, we have developed a detailed mechanistic understanding of these reactions under physiologically relevant conditions. We have revealed that Aβ42 fibril formation is inhibited by the binding of Aβ40, Aβ38 and Aβ37 to Aβ42 fibril surfaces, inhibiting secondary nucleation of new Aβ42 fibrils. We have also found that formation of co-oligomers of Aβ42 and Aβ40 is catalyzed by these same Aβ42 fibril surfaces. These co-oligomers ultimately produce fibrils consisting purely of Aβ40 peptides. Although no data are currently available to prove it, it seems highly likely both on physical chemistry grounds and by analogy with Aβ40 that the same holds for the formation of co-oligomers of Aβ42 and Aβ38/Aβ37.

V. Methods

Section V A introduces general rate equations that describe a wide range of protein aggregation reactions. In Section V B we nondimensionalize these rate equations and develop a divergent perturbative solution. In Section V C we explain why most standard approximate methods fail to produce a convergent solution. In the SI we therefore develop a new approximate method for solving differential equations dependent on a kind of Lie symmetry and use it to solve the general rate equations. In Section V D we describe qualitatively our method in a way that does not require knowledge of Lie symmetries or group theory, and present the resultant general solution formula for protein aggregation kinetics. In Section V E we apply this general solution formula to the coaggregation rate equations presented in the Results. Sections V F–V G outline the experimental techniques used to collect new coaggregation data, and how these data are subsequently processed. Finally, Section V H provides a reference table for notation used throughout the paper.

A. Generalized rate equations for protein fibril formation reactions

The kinetics of amyloid fibril self-assembly *in vitro* can typically be modelled by developing rate equations for the fibril number concentration $P(t)$, fibril mass concentration $M(t)$, and the monomer concentration $m(t)$. In the usual case that the aggregation reaction is "closed", and concentrations of oligomers or other intermediates is low, the total concentration $M(t) + m(t) = m_{\mathrm{tot}}$ of protein molecules in monomers and fibrils is constant to a good approximation.

Since amyloid fibrils typically contain a small number of monomers per plane, but a very large number of planes per fibril, their aggregation can be accurately modelled as a linear self-assembly reaction. New protein fibrils form from monomer

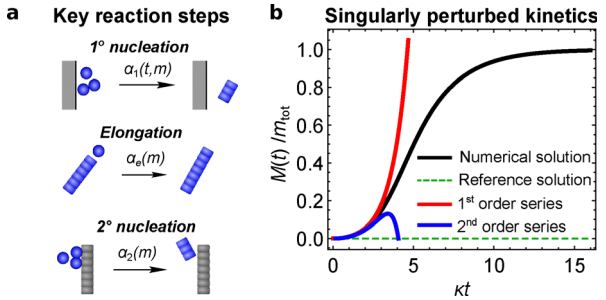

Fig. 6 Demonstration that the rate equations of standard protein aggregation reactions are singularly perturbed. (a) Types of reaction steps involved in standard reactions: initial nucleation of new fibrils (rate α_1); fibril elongation (rate α_e); autocatalytic secondary processes generating new fibrils (rate α_2), such as secondary nucleation (illustrated). (b) The numerically integrated general rate equations (eqn (12) normalized to $m(0)$, black) compared to the perturbative solutions. Parameters: $n_2 = 3$, $n_c = 2$, $\varepsilon = 0.01$, $\Pi(0) = 0$, $\mu(0) = 1$, and $\alpha_1 = \alpha_2 = \alpha_e = \text{const}$. After a short initial time period the first- and second-order perturbation series (eqn (15a), red and eqn (S43), blue) diverge from the numerically integrated kinetics.

in solution through a slow primary nucleation reaction step (often mediated by third-party interfaces such as the air–water interface or plate walls),[9,39–43] and subsequently elongate rapidly by monomer addition (Fig. 6a). Elongation does not create or remove fibrils and thus only affects $M(t)$ and $m(t)$ (decreasing the latter with rate proportional to $m(t)P(t)$). Since nucleation is much slower than elongation, the monomer lost during nucleation can be ignored and to a good approximation primary nucleation increases only $P(t)$ (with rate dependent only on monomer concentration).

Most amyloid-forming systems also feature reaction steps whose rates are proportional to the fibril mass concentration, sometimes summarised as multiplication processes or secondary processes. Such processes induce autocatalytic amplification in filamentous self-assembly. They include fibril fragmentation (rate $k\_M(t)$) as well as secondary nucleation of new fibrils on the surface of existing fibrils (Fig. 6a; rate dependent on both $m(t)$ and $M(t)$).

We wish to be as general as possible about amyloid kinetics in this paper, so we consider a general form for the kinetic equations that can also capture a range of more complex behaviours such as coaggregation, multi-step nucleation and enzyme-like saturation effects. This can be done by writing them in the form:

$$\frac{\mathrm{d}P}{\mathrm{d}t} = \alpha_1(t,m) + \alpha_2(m)M(t) \tag{11a}$$

$$\frac{\mathrm{d}M}{\mathrm{d}t} = \alpha_e(m)P(t). \tag{11b}$$

Here, $\alpha_1(t, m)$ is a general rate law for primary nucleation processes, depending on time t both explicitly and implicitly *via* $m(t)$. The simplest and most commonly studied example is the classical nucleation rate law $k_n m(t)^{n_c}$ (having no explicit t-dependence in this case), where k_n is the primary nucleation rate constant and $n_c \geq 0$ the monomer reaction order. Similarly, $\alpha_2 M$ and $\alpha_e P$ are general expressions for the rates of secondary processes and of elongation; since elongation is monomer-dependent, $\lim_{m\to m_c} \alpha_e = 2k_+(m - m_c)$, where m_c is the monomer solubility. The most simple and commonly studied instances of these rate laws are $\alpha_2(m) = k_2 m(t)^{n_2}$ and $\alpha_e(m) = 2k_+ m(t)$, where k_+ and k_2 are elongation and secondary process rate constants and $n_2 \geq 0$ the monomer reaction order for secondary processes. (When $n_2 = 0$ this rate law can also describe fragmentation.) For aggregation reactions (*i.e.* starting with an excess of monomer), α_1, α_e and α_2 are always >0.

Certain restrictions on the forms of these rates are necessary for the applicability of the Lie symmetry method we develop. First, α_2 and α_e must depend on constant parameters $\mathbf{d}$ in such a way that $\mathbf{d} = 0$ reduces them to $\alpha_2(m, \mathbf{d} = 0) = k_2 m^{n_2}$, and $\alpha_e(m, \mathbf{d} = 0) = 2k_+ m$. Many possible rate laws for elongation and secondary processes can be written in this way. For example, saturated elongation can be captured by this formalism with $\alpha_e = 2k_+ m(t)/(1 + m(t)/K_E)$.[9] Indeed, excepting those that explicitly model nonfibrillar oligomers, almost all previously discovered rate laws describing amyloid fibril formation are captured by these forms. Crucially, this restriction ensures that eqn (11) admits a special analytical solution (eqn (S30); derived in SI Section S2C) when $\mathbf{d} = \alpha_1(0, m_{\mathrm{tot}}) = 0$ and $P(0)$ is a particular function of $M(0)$. Although not useful in itself, its existence will later enable us to solve these equations generally. Second, defining $\varepsilon = \alpha_1(0, m_{\mathrm{tot}})/2m_{\mathrm{tot}}\alpha_2(m_{\mathrm{tot}})$, which can be interpreted as the relative importance of primary nucleation over secondary processes, we require that $\varepsilon \ll 0$. Third, we require that $\alpha_1(t, m_{\mathrm{tot}})$ must grow less rapidly with t than $\mathrm{e}^{\kappa t}$, where $\kappa = \sqrt{\alpha_e(m_{\mathrm{tot}})\alpha_2(m_{\mathrm{tot}})}$. The rationale for these latter two restrictions will be outlined below.

B. Fibril formation rate equations admit divergent perturbative solutions

An important first step for mathematical analysis of equations in general is to nondimensionalize them to remove their units. This often simplifies their structure and reduces the number of constants they depend on ref. 56. Defining $\mu = m(t)/m_{\mathrm{tot}}$ and $\kappa = \sqrt{\alpha_e(m_{\mathrm{tot}})\alpha_2(m_{\mathrm{tot}})}$, we can productively nondimensionalize and simplify eqn (1) using $\tau = \kappa t$ and $\Pi(t) = \alpha_e(m_{\mathrm{tot}})P(t)/m_{\mathrm{tot}}\kappa$, yielding:

$$\frac{\mathrm{d}\Pi}{\mathrm{d}\tau} = 2\varepsilon\frac{\alpha_1(t,m)}{\alpha_1(0,m_{\mathrm{tot}})} + \frac{\alpha_2(m)}{\alpha_2(m_{\mathrm{tot}})}(1 - \mu(\tau)) \tag{12a}$$

$$\frac{\mathrm{d}\mu}{\mathrm{d}\tau} = -\frac{\alpha_e(m)}{\alpha_e(m_{\mathrm{tot}})}\Pi(\tau). \tag{12b}$$

Eqn (12) cannot be solved exactly for $M(t)$, even in its simplest incarnation.[3,4] Nonetheless, since analytical solutions possess a number of advantages over numerical integration, accurate approximate solutions to these equations are of great value. Indeed, the greater clarity and simplicity can often make simple approximate solutions even more useful than exact solutions. Many techniques for obtaining globally valid approximate solutions to differential equations, including our technique, use perturbation theory as a starting point. This amounts

to looking for a series solution in a (usually small) parameter s entering the equations. For general differential equation $F(y, x, s, \mathrm{d}y/\mathrm{d}x, \mathrm{d}^2y/\mathrm{d}x^2, \ldots) = 0$, we would first make the substitution $y(x) = \sum_{i=0} s^i y^{(i)}(x)$ and then collect terms in powers of s. The equations at each order in s are often simpler than the original equation, permitting $y^{(0)}$, $y^{(1)}$, *etc* to be sequentially calculated. Even just the first two or three terms of this series can give an accurate approximate solution.

Writing the initial conditions as $\{\mu(0) = 1 - \delta, \Pi(0) = p\}$, eqn (12) admit a perturbation series in ε, δ and p. The restriction $\varepsilon \ll 1$ on the rate equations introduced above is now understood as ensuring the ability of such a perturbation series to approximately solve eqn (12). To simplify the perturbation calculations, we first replace these with $s\varepsilon$, $s\delta$ and sp, where s is a bookkeeping parameter to be later set to 1. We then expand eqn (12) in s, resulting in the following perturbation equations. At $O(s^0)$:

$$\frac{\mathrm{d}\Pi^{(0)}}{\mathrm{d}\tau} = \frac{\alpha_2\left(m_{\mathrm{tot}}\mu^{(0)}\right)}{\alpha_2(m_{\mathrm{tot}})}\left(1 - \mu^{(0)}\right), \quad \Pi^{(0)}(0) = 0, \tag{13a}$$

$$\frac{\mathrm{d}\mu^{(0)}}{\mathrm{d}\tau} = -\frac{\alpha_{\mathrm{e}}\left(m_{\mathrm{tot}}\mu^{(0)}\right)}{\alpha_{\mathrm{e}}(m_{\mathrm{tot}})}\Pi^{(0)}, \quad \mu^{(0)}(0) = 1. \tag{13b}$$

These can be solved by $\mu^{(0)}(\tau) = 1$, $\Pi^{(0)}(\tau) = 0$. The $O(s^1)$ equations are:

$$\frac{\mathrm{d}\Pi^{(1)}}{\mathrm{d}\tau} = 2\varepsilon\frac{\alpha_1(t, m_{\mathrm{tot}})}{\alpha_1(0, m_{\mathrm{tot}})} - \mu^{(1)}, \quad \Pi^{(1)}(0) = p \tag{14a}$$

$$\frac{\mathrm{d}\mu^{(1)}}{\mathrm{d}\tau} = -\Pi^{(1)}, \quad \mu^{(1)}(0) = -\delta. \tag{14b}$$

Provided $\alpha_1(t, m_{\mathrm{tot}})$ is integrable, this is solved by:

$$\mu^{(1)}(\tau) = -\left[\varepsilon\mathcal{F}(\tau) + \frac{\delta}{2}(\mathrm{e}^{\tau} + \mathrm{e}^{-\tau}) + \frac{p}{2}(\mathrm{e}^{\tau} - \mathrm{e}^{-\tau})\right] \tag{15a}$$

$$\Pi^{(1)}(\tau) = \varepsilon\dot{\mathcal{F}}(\tau) + \frac{\delta}{2}(\mathrm{e}^{\tau} - \mathrm{e}^{-\tau}) + \frac{p}{2}(\mathrm{e}^{\tau} + \mathrm{e}^{-\tau}), \tag{15b}$$

where $\mathcal{F}(\tau)$ satisfies $\mathcal{F}(0) = \dot{\mathcal{F}}(0) = 0$. The above-introduced restriction that $\alpha_1(t, m_{\mathrm{tot}})$ must grow less rapidly with t than $\mathrm{e}^{\kappa t}$ ensures further that $\lim_{\tau\to\infty} \mathcal{F}(\tau)\mathrm{e}^{-\tau} = c_\varepsilon$, with c_ε a positive constant. This is necessary to ensure that the leading-order terms in the second-order perturbation series will be proportional to $\mathrm{e}^{2\kappa t}$, which is an essential requirement for applicability of the Lie symmetry-based method to second order in s (see SI Section S3). In the common case that α_1 has no explicit time-dependence, $\mathcal{F}(\tau) = \mathrm{e}^{\tau} + \mathrm{e}^{-\tau} - 2$.

Perturbation series for nonlinear differential equations often only provide accurate solutions near where the initial or boundary conditions have been imposed. They are said to be singular, and diverge from the true solution away from the initial or boundary conditions. $\sum_i s^i\mu^{(i)}$ is an example of such singular perturbation series, being valid only asymptotically towards the phase point corresponding to the initial conditions (Fig. 6b). Unusually, however, whereas a typical singular perturbation series can be solved for arbitrary initial or boundary conditions, permitting this phase point to be moved arbitrarily, the region of validity of this series is instead fixed around $\{\mu(0) = 1, \Pi(0) = 0\}$, since these are the only initial conditions for which it solves eqn (13) and (14). We refer to such singular perturbation series, in which the initial or boundary conditions contain perturbation parameters, as "local perturbation series". (Note that a local perturbation series is not the same as a perturbation series in the independent variables, which is usually referred to as "local analysis".[57])

C. Failure of standard methods to generate convergent solutions

As mentioned in the Introduction, to date most widely-adopted convergent analytical solutions for the kinetics of protein aggregation reactions were derived using a technique called fixed-point theory.[3–6] As was also stated in the Introduction, fixed-point theory is unsuitable for solving the kinetic equations of most coaggregation reactions. Ultimately this comes down to the fact that most coaggregation reactions are dominated by different timescales at different times, as the composition of the reaction volume evolves. As outlined in SI Section S4A, fixed-point theory has great difficulty accounting efficiently for these timescale shifts.

Perhaps the most promising alternatives to fixed-point theory are so-called "singular perturbation methods". These are techniques that convert standard (divergent) singular perturbation series into globally valid (convergent) solutions. However, in a recent work[58] we demonstrated that the mathematical basis of many of the most popular and powerful singular perturbation methods, including Chen–Goldenfeld–Oono renormalization group (CGO RG), the method of multiple scales, and reductive perturbation, originates in certain symmetry properties of the differential equation's solution. At this stage we do not need to know the nature of these symmetry properties. The key relevant finding is that these techniques are valid only when these symmetry properties are inherited by the solution's singular perturbation series. This occurs only if the perturbation series can be made a valid series expansion of the exact solution at any point on the solution manifold by careful choice of the constants of integration. Consequently, such methods cannot be used here, since local perturbation series are valid series expansions of the exact solution only at one position on the manifold, for only one choice of the constants of integration. The apparent successful use of CGO RG to solve protein aggregation kinetics in certain prior studies[8,9] might appear to contradict this conclusion. However, in SI Section S4B we investigate these studies' derivations in depth and find that, although correct, they do not truly use CGO RG. Therefore, the RG formalism in these studies is superfluous and the apparent contradiction with our findings here is illusory.

D. General solution to the rate equations using Lie symmetries

Consequently, we have developed an alternative method based on the symmetry properties of the rate equations and their solutions. Its mathematical underpinnings are based on Lie group theory and its applications to differential equations. To increase the accessibility of our findings we relegate the method itself and its derivation to SI Section S2, and provide only a high-level

description here alongside the solution to the general rate equations. We also provide in SI Section S1 a brief review of those parts of the Lie group theory of differential equations that are needed to understand our results; see ref. 58 for a more detailed review.

The basic idea of the method is to symmetry-transform a known special solution to eqn (12), valid for specific choices of the constant parameters entering the equations and their initial conditions, into a general solution valid for *any* parameter values. As stated above, such a solution (eqn (S30)) is available for eqn (11) (or equivalently eqn (12)). The procedure for transforming this special solution into a general one can be derived from Lie group theory by considering a type of symmetry called an "asymptotic symmetry". It is fundamentally different from the class of symmetries underlying the most popular singular perturbation techniques mentioned above, which are instead known as "approximate Lie symmetries".[58,59]

Using this method, the formula for the general solution to protein aggregation rate equations of the form eqn (11) is found in SI Section S3 to be:

$$M(t) = m_{\mathrm{tot}} - m_{\mathrm{tot}}\left(1 - \frac{\mu^{(1)}(\kappa t)}{c_1}\right)^{-c_1} \tag{16a}$$

$$\kappa = \sqrt{\alpha_e(m_{\mathrm{tot}})\alpha_2(m_{\mathrm{tot}})} \tag{16b}$$

$$c_1 = \frac{3}{2n_2' + 1}, \quad n_2' = \left.\frac{d\ln\left[\alpha_2(m)\alpha_e(m)^2\right]}{d\ln m}\right|_{m=m_{\mathrm{tot}}} - 2, \tag{16c}$$

and $\mu^{(1)}$ is the solution, eqn (15a), to the first order perturbation equation, eqn (14).

There is one further condition that needs to be met for the applicability of our method, and therefore the validity of eqn (16), beyond the aforementioned restrictions on the rate terms entering eqn (11). In technical terms, this condition is that the asymptotic symmetry underlying the method is approximately valid globally in the parameter space of interest (see SI Section S2B for a technical explanation). In practical terms, this means that eqn (16) is only applicable to aggregation reactions that fall into one of two general classes. These can be expressed without discussing Lie symmetries as follows. First, if the parameters $\mathbf{d}$ drop out of the $\mu \to 0$ kinetics at leading order and the parameters (ε, p, δ) are small. Most unsaturated single-protein aggregation reactions with low or no seeding fall into this class, as do the coaggregation reactions studied here when unsaturated (see SI Section S4C). The second class is kinetic equations for which the rate of nucleation remains large until late reaction times. Most reactions featuring saturation of secondary nucleation, including the coaggregation reactions studied here, fall into this second class (see SI Section S4C). Unsaturated, highly seeded aggregation reactions (where $M(0)/m_{\mathrm{tot}}$ or $\alpha_e(m_{\mathrm{tot}})P(0)/m_{\mathrm{tot}}\kappa$ are not small) or reactions with slow secondary processes (*i.e.* ε is not small) fall into neither class; its treatment by asymptotic symmetry methods requires an extension of the methodology explored in a follow-on paper.[53]

E. Application of the general solution formula to the Aβ42–Aβ*xx* rate equations

1. Aβ42 fibril formation. Identifying $\mathbf{d}_a = (m_{\mathrm{tot},a}/K_{\mathrm{S}}(a), m_{\mathrm{tot},b}/K_{\mathrm{S}}(ba))$ shows that $\alpha_{e,a}$ and $\alpha_{2,a}$ are of the form required for applicability of the general solution formula (eqn (16)) to the Aβ42 rate equations (eqn (1)–(3)). Since $\alpha_{1,a}$ has no explicit time-dependence, it too is of the correct form (these forms are explained in Methods Section V A). The nondimensional general protein aggregation rate equations (eqn (12)), and consequently their first-order perturbative solution, can therefore be mapped to eqn (1)–(3) by addition of subscripts a to all terms and identification of τ as $\kappa_a t$. Since $\alpha_{1,a}$ has no explicit time-dependence, we can immediately write down $\mu_a^{(1)}$ using eqn (15a):

$$\mu_a^{(1)} = -\left[\varepsilon_a\left(\mathrm{e}^{\kappa_a t} + \mathrm{e}^{-\kappa_a t} - 2\right) + \frac{\delta_a}{2}\left(\mathrm{e}^{\kappa_a t} + \mathrm{e}^{-\kappa_a t}\right) + \frac{p}{2}\left(\mathrm{e}^{\kappa_a t} - \mathrm{e}^{-\kappa_a t}\right)\right], \tag{17}$$

where:

$$p_a = \Pi_a(0) = \frac{\alpha_{e,a}\left(m_{\mathrm{tot},a}\right)P_a(0)}{m_{\mathrm{tot},a}\kappa_a} \tag{18a}$$

$$\delta_a = 1 - \mu_a(0) = \frac{M_a(0)}{m_{\mathrm{tot},a}}. \tag{18b}$$

The general solution formula (eqn (16)) can be mapped in the same way, by addition of subscripts a to all terms. Its calculation therefore requires calculation of $n_2'(a)$. This requires evaluation of the quantity $\ln[\alpha_{2,a}(m_a)\alpha_{e,a}(m_a)^2]$, with $\alpha_{e,a}(m_a)$ and $\alpha_{2,a}(m_a)$ given by eqn (2) and (3). This is:

$$\text{const.} + \ln\left[\frac{\mathrm{e}^{(n_2(a)+2)\ln m_a}}{1 + \mathrm{e}^{n_2(aa)\ln m_a} m_{\mathrm{tot},b}^{n_2(ab)} \Big/ K_{\mathrm{S}}(ba)^{n_2(aa)+n_2(ab)} + \mathrm{e}^{n_2(a)\ln m_a}/K_{\mathrm{S}}(a)^{n_2(a)}}\right]. \tag{19}$$

Differentiating with respect to $\ln m_a$ gives eqn (20) which gives in turn eqn (21) for $n'_2(a)$.

$$\left.\frac{d\ln\left[\alpha_{2,a}(m_a)\alpha_{e,a}(m_a)^2\right]}{d\ln m_a}\right|_{m_a=m_{\mathrm{tot},a}} = n_2(a) + 2 - \frac{n_2(a)\left(m_{\mathrm{tot},a}/K_{\mathrm{S}}(a)\right)^{n_2(a)} + n_2(aa)\left(m_{\mathrm{tot},a}/K_{\mathrm{S}}(ba)\right)^{n_2(aa)}\left(m_{\mathrm{tot},b}/K_{\mathrm{S}}(ba)\right)^{n_2(ab)}}{1 + \left(m_{\mathrm{tot},a}/K_{\mathrm{S}}(ba)\right)^{n_2(aa)}\left(m_{\mathrm{tot},b}/K_{\mathrm{S}}(ba)\right)^{n_2(ab)} + \left(m_{\mathrm{tot},a}/K_{\mathrm{S}}(a)\right)^{n_2(a)}}. \tag{20}$$

$$\begin{aligned} n_2'(a) \;=\; & n_2(a)\frac{1 + \left(m_{\mathrm{tot},a}/K_{\mathrm{S}}(ba)\right)^{n_2(aa)}\left(m_{\mathrm{tot},b}/K_{\mathrm{S}}(ba)\right)^{n_2(ab)}}{1 + \left(m_{\mathrm{tot},a}/K_{\mathrm{S}}(ba)\right)^{n_2(aa)}\left(m_{\mathrm{tot},b}/K_{\mathrm{S}}(ba)\right)^{n_2(ab)} + \left(m_{\mathrm{tot},a}/K_{\mathrm{S}}(a)\right)^{n_2(a)}} \\ & - n_2(aa)\frac{\left(m_{\mathrm{tot},a}/K_{\mathrm{S}}(ba)\right)^{n_2(aa)}\left(m_{\mathrm{tot},b}/K_{\mathrm{S}}(ba)\right)^{n_2(ab)}}{1 + \left(m_{\mathrm{tot},a}/K_{\mathrm{S}}(ba)\right)^{n_2(aa)}\left(m_{\mathrm{tot},b}/K_{\mathrm{S}}(ba)\right)^{n_2(ab)} + \left(m_{\mathrm{tot},a}/K_{\mathrm{S}}(a)\right)^{n_2(a)}}. \end{aligned} \tag{21}$$

$$\mu_b^{(1)} \simeq \frac{\alpha_{1,bb}(m_{\mathrm{tot},b}) + f_1\alpha_{1,ba}(m_{\mathrm{tot},a}, m_{\mathrm{tot},b}) + f_2 m_{\mathrm{tot},a}\alpha_{2,ba}(m_{\mathrm{tot},a}, m_{\mathrm{tot},b})}{2m_{\mathrm{tot},b}\alpha_{2,b}(m_{\mathrm{tot},b})}(e^{\kappa_b t} + e^{-\kappa_b t} - 2) \quad (23a)$$

In concert with the expression for $\mu_a^{(1)}$ derived above (eqn (17)), we can then write down the following analytical solution to the Aβ42 rate equations:

$$\frac{M_a(t)}{m_{\mathrm{tot},a}} = 1 - \left[1 + \frac{\delta_a}{2c_a}(e^{\kappa_a t} + e^{-\kappa_a t}) + \frac{p_a}{2c_a}(e^{\kappa_a t} - e^{-\kappa_a t}) + \frac{\varepsilon_a}{c_a}(e^{\kappa_a t} + e^{-\kappa_a t} - 2)\right]^{-c_a}, \quad (22a)$$

$$c_a = \frac{3}{2n_2'(a) + 1}. \quad (22b)$$

When $\delta_a = p_a = 0$, this reduces to eqn (7). We validate this solution against numerical integration in Fig. 7a, finding it to be highly accurate.

2. Aβxx fibril formation. Identifying $\mathbf{d}_b = m_{\mathrm{tot},b}/K_S(b)$ shows that $\alpha_{e,b}$ and $\alpha_{2,b}$ are also of the form required for applicability of the general solution formula (eqn (16)) to the Aβxx rate equations (eqn (4)). Although $\alpha_{1,b}$ now has explicit time-dependence, it shrinks with time on the timescale of $\kappa_b t$; therefore, it too is of the correct form (these forms are explained in Methods Section V A). Eqn (4) can therefore be mapped to the nondimensional general protein aggregation rate equations (eqn (12)), and consequently their associated perturbation equations (eqn (13) and (14)), by addition of subscripts b to all terms and identification of τ as $\kappa_b t$. However, the explicit time-dependence of $\alpha_{1,b}$ causes the function $\mathcal{F}$ entering the first order perturbation solution, eqn (15a), to be very complex. Fortunately it can be extensively simplified (SI Section S6), giving finally:

$$f_1 = 1 - \left(\frac{2\varepsilon_a + \delta + p}{2c_a}\right)^{\frac{\kappa_b}{\kappa_a}} \bar{f}_1, \quad f_2 = \left(\frac{2\varepsilon_a + \delta + p}{2c_a}\right)^{\frac{\kappa_b}{\kappa_a}} \bar{f}_2, \quad (23b)$$

where

$$\bar{f}_1 = h(n_c(ba)), \quad \bar{f}_2 = (h(n_2(ba) + 1) - h(n_2(ba))), \quad (24a)$$

$$h(x) = {}_2F_1\left[-\frac{\kappa_b}{\kappa_a}, 1 - \frac{\kappa_b}{\kappa_a} - c_a x, 1 - \frac{\kappa_b}{\kappa_a}, 1\right], \quad (24b)$$

and ${}_2F_1[\ldots]$ is the Gaussian hypergeometric function.

Adding subscripts b, use of the general solution formula eqn (16) for M_b requires calculation first of $n_2'(b)$. This in turn requires evaluation of $\ln[\alpha_{2,b}(m_b)\alpha_{e,b}(m_b)^2]$. Using eqn (5), this is:

$$\ln\left[\alpha_{2,b}(m_b)\alpha_{e,b}(m_b)^2\right] = \text{const.} + \ln\left[\frac{e^{(n_2(b)+2)\ln m_b}}{1 + e^{n_2(b)\ln m_b}/K_S(b)^{n_2(b)}}\right]. \quad (25)$$

Differentiating with respect to $\ln m_b$ gives:

$$\left.\frac{d\ln\left[\alpha_{2,b}(m_b)\alpha_{e,b}(m_b)^2\right]}{d\ln m_b}\right|_{m_b = m_{\mathrm{tot},b}} = n_2(b) + 2 - \frac{n_2(b)\left(m_{\mathrm{tot},b}/K_S(b)\right)^{n_2(b)}}{1 + \left(m_{\mathrm{tot},b}/K_S(b)\right)^{n_2(b)}}. \quad (26)$$

So:

$$n_2'(b) = n_2(b)\frac{1}{1 + \left(m_{\mathrm{tot},b}/K_S(b)\right)^{n_2(b)}}. \quad (27)$$

Putting this all together, eqn (16) then immediately gives eqn (8) for $M_b(t)$. This solution too corresponds closely to the numerically integrated rate equations (Fig. 7b).

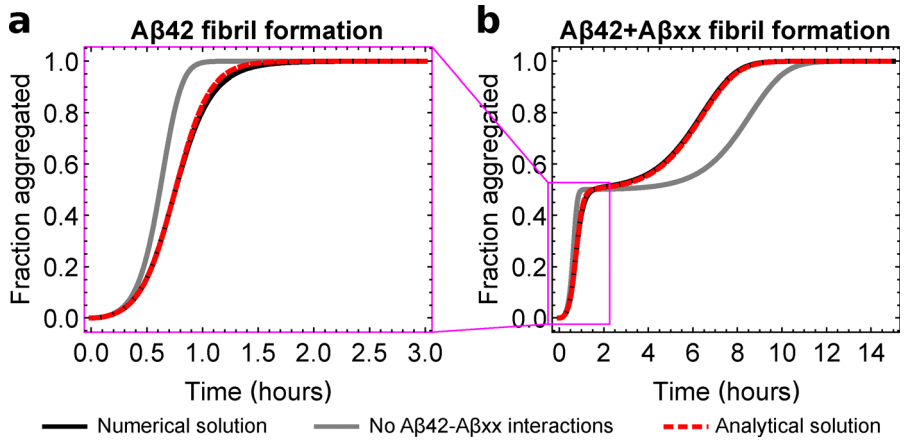

Fig. 7 Analytical solutions to the kinetics of Aβ42–Aβxx coaggregation (red, dashed) are highly accurate, tracking the numerical solutions to the rate equations (black) almost exactly. Monomer concentrations are 4 μM of each; rate constants are those subsequently determined by fitting experimental data for Aβ40–Aβ42 coaggregation (see Table S6). Numerical solutions in the absence of Aβ42–Aβxx interactions (gray) show a clear difference. (a) The analytical solution to the kinetics of self-assembly of Aβ42 fibrils in the presence of Aβ40 monomers (eqn (7)) closely tracks the numerical solution to eqn (1)–(3). (b) Kinetics of self-assembly of all fibrils together are modelled accurately by the combined analytical solution eqn (10), implying that Aβ40 fibrils (rate equations eqn (4)–(6)) are similarly well-described by the analytical solution eqn (8).

F. Experimental methods

1. Chemicals and consumables. Unless otherwise specified, the experimental buffer used is always 20 mM sodium phosphate, 0.2 mM EDTA at pH 7.4. The buffers used were always filtered through water-wettable polytetrafluoroethylene (0.22 μm, 60539, Pall corporation) and degassed prior to use. ThT was purchased from CalBiochem and stock solution filtered (0.2 μm) before use.

2. Expression & purification of Aβ variants. The sequences for Aβ (M1–42), Aβ (M1–40), Aβ (M1–38) and Aβ (M1–37) referred to in this work as Aβ42, Aβ40, Aβ38 and Aβ37 were prepared using overlapping polymerase chain reaction and cloned in PetSac plasmid as reported in ref. 60 and 31, see ref. 61 for detailed protocol. In brief, the peptides were expressed in *Escherichia coli*, strain BL21 Star (DE3) pLysS for Aβ42 and Aβ (M1–37), BL21-Gold (DE3) pLysS (Invitrogen, Waltham, MA, USA) for Aβ38 and T7 Express (New England Biolabs, Ipswich, MA, USA) was used for Aβ (M1–40). After harvesting and lysis of the cells, the peptide was isolated from inclusion bodies through a series of ion-exchange and size-exclusion chromatography steps.[61] Aliquots of the purified proteins were lyophilised and kept frozen until further use.

3. Isolation of monomers. Prior to each kinetic experiment, a freeze-dried peptide aliquot was reconstituted in 1 mL 6 M guanidine hydrochloride and subjected to separation on a 10/300 Superdex 75 increase, size exclusion column. This was done to ensure the highest possible degree of homogeneous monomer at the start of each experiment. The monomers were isolated in the desired experimental buffer and their concentration was determined by integration of the chromatogram monitored at 280 nm and calculated using Beer's law, using an extinction coefficient of 1490 M^{-1} cm^{-1}.

4. Aggregation kinetics. Aggregation kinetics were followed by monitoring the increase of fibril mass through the fluorescence intensity of 5 μM ThT with excitation at 448 nm and emission at 480 nm. The reactions were performed with 100 μL in each well (3881, Corning, USA) in a FLUOstar Omega (BMG LABTECH).

G. Data processing

The data displayed in Fig. 7A of ref. 30 exhibits relatively high variability between replicates in the half-time of the second sigmoid, corresponding to Aβ40 aggregation. Plotting all replicates visually obscures the trend in half time *versus* Aβ42 seed concentration for this transition. Some of this variability originates from variability in ThT fluorescence, as evident from the large spread in values for the first ThT plateau's relative height. Since the direction of this trend is important in determining the mechanism of coaggregation, we performed some additional data processing steps prior to re-plotting these curves and fitting our kinetic models to them.

First, each curve was divided into two time portions, each containing one of the two sigmoids. This allowed us to normalize each sigmoid independently, and to remove certain large jumps or discontinuities between adjacent time points that are clearly artefactual. The two portions were then recombined with appropriate normalization factors to ensure that the recombined curves reflect relative fibril mass concentration. This processing step already reduced the variability in the half time for the second sigmoid, although still larger than desired.

As a second step, we retained only the replicates with the median second-sigmoid half time for each condition. For conditions with even numbers of replicates, we averaged over the two curves with median half-times. The resulting curves, displayed in Fig. 3a and b, are much more easily interpretable than the raw data displayed in ref. 30. Note, comparatively little variability is evident in the half-times of the first sigmoid prior to removing these replicates.

We performed identical data processing methodology for the kinetic curves measured in the fresh experiments we performed ourselves as part of this study. These are displayed in Fig. 3c and d.

H. Summary of notation used in this study

Table 1

Table 1 Chemical and mathematical notation used throughout the paper

Parameter	Definition	Typical value
x_a, $x(a)$	Parameter x pertaining to faster-aggregating species a	N/A
x_b, $x(b)$	Parameter x pertaining to slower-aggregating species b	N/A
k_n	1° nucleation rate constant	$0.01/k_+$ μM^{-n_c+1} h^{-1}
k_2	2° nucleation rate constant	$10/k_+$ μM^{-n_2} h^{-1}
k_+	Elongation rate constant	$10/k_2$ μM^{-1} h^{-1}
n_c	1° nucleation reaction order	2
n_2	2° nucleation reaction order	2
m_{tot}	Total monomer concentration	3 μM
K_S	Dissociation constant for monomers from fibril surfaces	1 μM
$\mathcal{K}_S = K_S/m_{tot}$	Nondimensionalized dissociation constant	0.25
$\alpha_1(m)$	Primary nucleation rate	$0.1/k_+$ μM h^{-1}
$\alpha_2(m)$	Secondary nucleation rate	$10/k_+$ h^{-1}
$\alpha_e(m)$	Elongation rate	$30/k_2$ h^{-1}
$\kappa = \sqrt{\alpha_e(m_{tot})\alpha_2(m_{tot})}$	Rate of proliferation of fibrils by secondary processes	5 h^{-1}
$\varepsilon = \alpha_1(m_{tot})/2m_{tot}\alpha_2(m_{tot})$	Rate of secondary vs primary nucleation	0.01
$\tau = \kappa t$	Nondimensionalized time	3
$\mu(\tau) = m(\tau)/m_{tot}$	Nondimensionalized monomer concentration	$0 \leq \mu \leq 1$
$\Pi(\tau) = 2k_+P(\tau)/\kappa$	Nondimensionalized fibril concentration	$\approx 1 - \mu$
$1 - \delta$	Initial dimensionless monomer concentration	0.98
p	Initial dimensionless fibril concentration	0.02
s	Perturbation indexing parameter	N/A

Author contributions

Conceptualization: AJD, LM. Data curation: AJD, EA, XY, RC. Formal analysis: AJD. Funding acquisition: LM, SL, AJD, TCTM. Investigation: AJD, EA, XY, RC. Methodology: AJD, GM. Project administration: AJD, SL, LM. Software: AJD, GM. Supervision: AJD, TCTM, SL, LM. Visualization: AJD, GM. Writing – original draft: AJD, GM. Writing – review and editing: AJD, GM, TCTM, SL, LM.

Conflicts of interest

There are no conflicts to declare.

Data availability

Data for this article, including all raw data and data processing, are available at figshare at **https://doi.org/10.6084/m9.figshare.28722848**.

Supplementary information is available. The contents of the SI are described in the final paragraph of the introduction. See DOI: **https://doi.org/10.1039/d5cp01288k**.

Appendices

A Derivation of general rate law for saturating and inhibited secondary nucleation

As discussed at length in the literature,[6,9,45,52] secondary nucleation in amyloid-β formation is well-modelled as the co-operative binding of two or more monomers to a catalytic site on fibril surfaces, and their subsequent conversion to a new fibril nucleus. The rate-limiting step of this conversion reaction pathway must be monomer-independent for Michaelis–Menten-like saturation effects to be observed in the secondary nucleation rate. If Aβ*xx* monomers can inhibit Aβ42 secondary nucleation specifically, without also affecting primary nucleation, then this inhibition must be achieved competitively, by their also binding to secondary nucleation sites on the Aβ42 fibrils. What is not clear *a priori* is whether or not this binding is also co-operative, requiring multiple Aβ*xx* monomers or even a mixture of Aβ42 and Aβ*xx* monomers.

We will denote the conversion-competent clusters of Aβ42 monomers bound to catalytic sites on Aβ42 fibrils as M_a^*. For generality we will allow them to be of arbitrary minimum size $n_2(a)$. We will denote the Aβ*xx*-containing species bound to such sites as M_a^I. These consist predominantly of $n_2(aa)$ Aβ42 monomers and $n_2(ab)$ Aβ*xx* monomers, with these numbers to be determined later. Finally, we write M_a^f as the concentration of free (unbound) catalytic sites. The total mass concentration of Aβ42 fibrils can then be written as:

$$M_a = s_a\left(M_a^f + M_a^* + M_a^I\right), \tag{A1}$$

where s_a is the stoichiometry of secondary nucleation sites, specifically, the number of monomeric subunits in a fibril per secondary nucleation site.

As discussed at length in previous publications,[6,9] Michaelis–Menten-type kinetics are a reasonable approximation to make for secondary nucleation in amyloid formation. Therefore, we make the simplifying assumption of pre-equilibrium or partial-equilibrium between bound and unbound states in the timescale of protein aggregation, *i.e.*:

$$\frac{m_a^{n_2(a)}M_a^f}{M_a^*} = K_S(a)^{n_2(a)}, \quad \frac{m_a^{n_2(aa)}m_b^{n_2(ab)}M_a^f}{M_a^I} = K_S(ba)^{n_2(aa)+n_2(ab)}, \tag{A2}$$

where $K_S(a)^{n_2(a)}$ and $K_S(ba)^{n_2(aa)+n_2(ab)}$ are the equilibrium dissociation constants for the unbinding of pure-Aβ42 clusters and of Aβ*xx*-containing species from the catalytic sites. Note, if $n_2(aa) = 0$ and $n_2(ba) = 1$, this is just the dissociation constant for Aβ*xx* monomers from a secondary nucleation site on an Aβ42 fibril.

Combining these equations allows us to express the total Aβ42 fibril mass concentration as:

$$M_a = s_a M_a^f\left(1 + (m_a/K_S(a))^{n_2(a)} + (m_a/K_S(ba))^{n_2(aa)}(m_b/K_S(ba))^{n_2(ab)}\right). \tag{A3}$$

Since we have seen that the presence of Aβ*xx* protein does not accelerate the aggregation of Aβ42, rates of conversion of mixed clusters to Aβ42 fibrils must be far slower than that of homogeneous Aβ42 clusters. Therefore, to a good approximation the rate of generation of new Aβ42 fibrils by secondary nucleation is:

$$r_S = 2k_c M_a^* = 2k_c M_a^f (m_a/K_S(a))^{n_2(a)}, \tag{A4}$$

where k_c is some conversion rate constant, this ultimately yields:

$$r_S = \frac{2k_2(a)m_a(t)^{n_2(a)}M_a(t)}{1 + (m_a(t)/K_S(a))^{n_2(a)} + (m_a/K_S(ba))^{n_2(aa)}(m_b/K_S(ba))^{n_2(ab)}}, \tag{A5}$$

where $k_2 = k_c/s_a K_S(a)^{n_2(a)}$. We are additionally at liberty in the present context to set $m_b = m_b(0)$ because Aβ42 aggregation is completed before significant depletion of Aβ*xx* monomers. Doing so yields finally eqn (3).

B Global fitting to determine the species causing inhibition

If competitive inhibition is caused by a single Aβ*xx* monomer binding to a secondary nucleation site on an Aβ42 fibril, then $n_2(aa) = 0$ and $n_2(ab) = 1$. Consequently, the expression for $\alpha_{2,a}$ becomes:

$$\alpha_{2,a}(m_a) = \frac{2k_2(a)m_a(t)^{n_2(a)}M_a(t)}{1 + (m_a(t)/K_S(a))^{n_2(a)} + (m_b(0)/K_S(ba))}. \tag{B1}$$

If instead two Aβ*xx* monomers must bind co-operatively to the nucleation site (*i.e.* $n_2(aa) = 0$ and $n_2(ab) = 2$), similarly to Aβ42, then homogenous clusters are the dominant species causing inhibition, and $\alpha_{2,a}$ is:

$$\alpha_{2,a}(m_a) = \frac{2k_2(a)m_a(t)^{n_2(a)}M_a(t)}{1 + (m_a(t)/K_S(a))^{n_2(a)} + (m_b(0)/K_S(ba))^{n_2(ab)}}. \tag{B2}$$

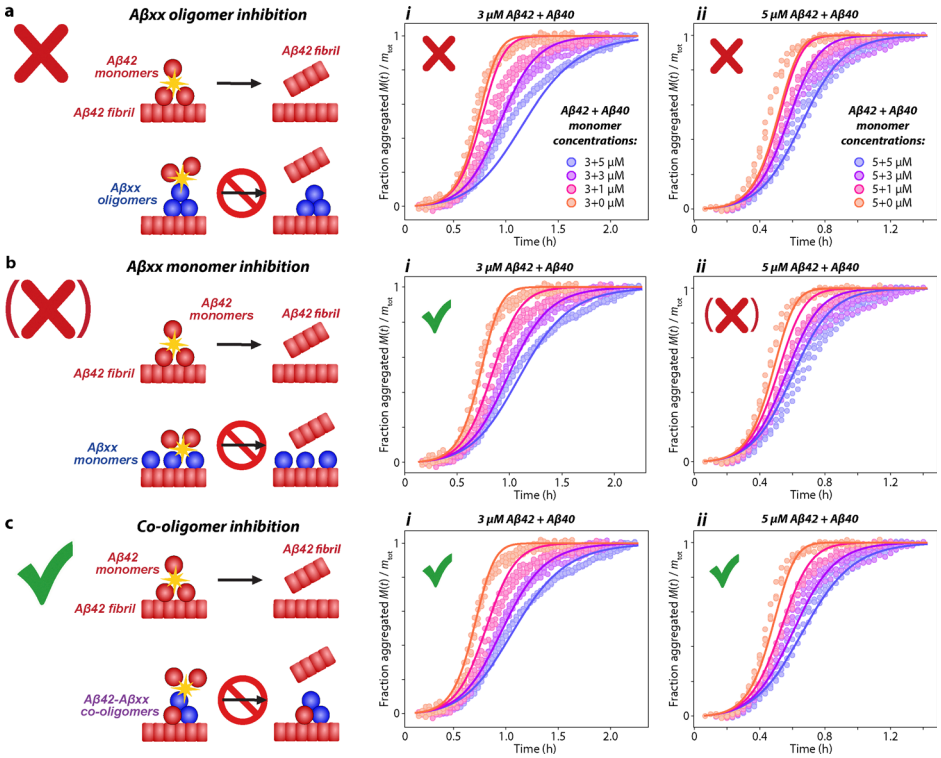

Fig. 8 In-depth kinetic analysis of the competitive inhibition of Aβ42 secondary nucleation by Aβ40-containing species attached to fibril surfaces provides further evidence of co-oligomer formation. Monomeric Aβ42 (i: 3 μM; ii: 5 μM) was aggregated with various initial Aβ40 monomer concentrations. Kinetic model used for fitting is eqn (7) with $K_E(ba)^{-1} = K_P(ba)^{-1} = 0$ throughout. (a) Global misfits of model in which pure-Aβ40 oligomers are the dominant cause of inhibition ($n_2(aa) = 0$ and $n_2(ab) = 2$). Mean residual errors (MREs) are 4.9×10^{-3} (i), 4.3×10^{-3} (ii). (b) Global fits of model in which monomeric Aβ40 are the dominant cause of inhibition ($n_2(aa) = 0$ and $n_2(ab) = 1$). MREs are 1.8×10^{-3} (i), 3.1×10^{-3} (ii). (c) Global fits of model in which Aβ42–Aβ40 co-oligomers are the dominant cause of inhibition ($n_2(aa) = 1$ and $n_2(ab) = 1$). MREs are 2.1×10^{-3} (i), 1.9×10^{-3} (ii). Fitted parameter values are summarized in Table S1. The improvement in fit quality from b to c is arguably insufficient to eliminate the monomeric-Aβ40 inhibition mechanism with high confidence. (Brackets around the misfit "X" symbol indicate when the MREs are slightly less than double those achieved with the model used in c.) However, in concert with the finding that co-oligomer formation on Aβ42 fibril surfaces drives the acceleration in Aβ40 fibril formation, it becomes highly likely that these co-oligomers also cause the inhibition of Aβ42 fibril formation, as opposed to some other species.

Note that with our Aβ*xx*–Aβ42 system it has been shown[30,31] that secondary nucleation of Aβ*xx* fibrils does not occur on Aβ42 fibrils, so clusters of Aβ*xx* monomers are unlikely to form on Aβ42 fibrils, making this possibility unlikely. Finally, if an Aβ*xx* can only bind to the nucleation site co-operatively with an Aβ42 monomer, then mixed clusters dominate inhibition. Arguably the simplest possible rate law for this involves assuming the same overall reaction order as for homogeneous nucleation, *i.e.* $n_2(aa) + n_2(ab) = n_2(a) = 2$, and equal dependence of the rate on the concentrations of each type of monomer, *i.e.* $n_2(aa) = n_2(ab)$. Overall, then, $n_2(aa) = n_2(ab) = 1$, and $\alpha_{2,a}$ is:

$$\alpha_{2,a}(m_a) = \frac{2k_2(a)m_a(t)^{n_2(a)}M_a(t)}{1+(m_a(t)/K_S(a))^{n_2(a)}+m_a(0)m_b(0)/K_S(ba))^2}. \quad \text{(B3)}$$

In Results Section II B it was determined that Aβ*xx* slows down Aβ42 aggregation by inhibiting its secondary nucleation, *i.e.* $K_S(ba) \neq 0$. This was done by globally fitting the rate laws for different inhibition targets to experimental kinetic curves for reactions featuring 3 μM of Aβ42 and varying concentrations of Aβ*xx* (Fig. 2). $n_2(ab)$ was explicitly fitted and found to be approximately 1. Conversely, since only one Aβ42 monomer concentration was used, $n_2(aa)$ could not be fitted. In our initial analysis it was therefore set arbitrarily to 0, *i.e.* eqn (B1) was initially used for fitting.

In this Appendix we fit eqn (7) globally to an expanded dataset for Aβ42–Aβ40 coaggregation (Fig. 8). Alongside 3 μM Aβ42 monomer, this includes previously-unpublished kinetic curves for reactions with 5 μM Aβ42 monomer (and the same range of Aβ40 concentrations as in Fig. 2). This allows us to verify that $n_2(ab) = 1$ and to additionally estimate the value of $n_2(aa)$. (The experiments involving 5 μM Aβ42 monomer were performed contemporaneously with those involving 3 μM Aβ42 monomer during the preparation of ref. 30. However, since kinetic model fitting was not thought possible at the time, the former experiments were ultimately deemed superfluous to the goals of the study and were therefore omitted from the publication).

We first confirm that $n_2(ab) = 1$ and that therefore pure-Aβ40 clusters do not inhibit Aβ42 secondary nucleation, finding that using eqn (B2) for $\alpha_{2,a}$ in our integrated rate law (eqn (7)) gives poor fits to this expanded dataset (Fig. 8a). We next test the possibility that binding of individual Aβ40 monomers to fibrils causes the inhibition, by fitting our integrated rate law eqn (7)

using eqn (B1) for $\alpha_{2,a}$. This gives fits of moderate quality but that somewhat overestimates the extent of inhibition for reactions with 3 μM Aβ42 and underestimates it for reactions with 5 μM Aβ42 (Fig. 8b).

Finally, we test the possibility that the inhibition is caused by the competition between Aβ42–Aβ40 co-oligomer formation with homogeneous Aβ42 oligomer formation on the fibril surface by using eqn (B3) for $\alpha_{2,a}$ in our integrated rate law. This gives almost perfect fits (Fig. 8c); however, on its own, the improvement in fit quality over Fig. 8b is insufficient to confirm this mode of action and rule out that the competitive inhibition is caused by monomeric Aβ*xx*. It should instead be viewed as a piece of evidence of moderate strength in favour of the formation of Aβ42–Aβ40 co-oligomers at the nucleation sites on Aβ42 fibrils in competition with pure-Aβ42 oligomers.

Given the apparent commonality in the effects of Aβ38 and Aβ37 on Aβ42 aggregation and *vice versa*, it is also more likely than not that this inhibitory mechanism applies to Aβ42–Aβ*xx* coaggregation more generally, not just for Aβ42–Aβ40 coaggregation. We therefore use eqn (B3) for all subsequent data fitting and for calculation of $K_S(ab)$. Note, the likelihood of this mechanism being correct is greatly increased by our subsequent discovery that formation of Aβ42–Aβ*xx* co-oligomers on Aβ42 fibrils also drives the acceleration of Aβ*xx* fibril formation.

Acknowledgements

We acknowledge support from the Lindemann Trust Fellowship, English-Speaking Union (AJD), the Swiss National Science Foundation (grant no 219703, AJD, TCTM), the Swedish Research Council (SL), the MacArthur Foundation (LM), the Simons Foundation (LM) and the Henri Seydoux Fund (LM). The research leading to these results has received funding from the European Research Council under the European Union's Seventh Framework Programme (FP7/2007–2013) through the ERC grants PhysProt (agreement no. 337969), MAMBA (agreement no. 340890) and NovoNordiskFonden (SL).

References

1 F. Chiti and C. M. Dobson, *Annu. Rev. Biochem.*, 2006, **75**, 333.
2 F. Chiti and C. M. Dobson, *Annu. Rev. Biochem.*, 2017, **86**, 27pMID: 28498720.
3 T. P. J. Knowles, C. A. Waudby, G. L. Devlin, S. I. A. Cohen, A. Aguzzi, M. Vendruscolo, E. M. Terentjev, M. E. Welland and C. M. Dobson, *Science*, 2009, **326**, 1533.
4 S. I. A. Cohen, M. Vendruscolo, M. E. Welland, C. M. Dobson, E. M. Terentjev and T. P. J. Knowles, *J. Chem. Phys.*, 2011, **135**, 065105.
5 S. I. A. Cohen, M. Vendruscolo, C. M. Dobson and T. P. J. Knowles, *J. Chem. Phys.*, 2011, **135**, 065106.
6 G. Meisl, X. Yang, E. Hellstrand, B. Frohm, J. B. Kirkegaard, S. I. A. Cohen, C. M. Dobson, S. Linse and T. P. J. Knowles, *Proc. Natl. Acad. Sci. U. S. A.*, 2014, **111**, 9384.
7 T. C. T. Michaels, S. I. A. Cohen, M. Vendruscolo, C. M. Dobson and T. P. J. Knowles, *Phys. Rev. Lett.*, 2016, **116**, 038101.
8 T. C. T. Michaels, A. J. Dear and T. P. J. Knowles, *Phys. Rev. E*, 2019, **99**, 062415.
9 A. J. Dear, G. Meisl, T. C. T. Michaels, M. R. Zimmermann, S. Linse and T. P. J. Knowles, *J. Chem. Phys.*, 2020, **152**, 045101.
10 G. Meisl, J. B. Kirkegaard, P. Arosio, T. C. T. Michaels, M. Vendruscolo, C. M. Dobson, S. Linse and T. P. J. Knowles, *Nat. Protoc.*, 2016, **11**, 252.
11 P. Arosio, T. P. J. Knowles and S. Linse, *Phys. Chem. Chem. Phys.*, 2015, **17**, 7606, DOI: **10.1039/C4CP05563B**.
12 G. Meisl, C. K. Xu, J. D. Taylor, T. C. T. Michaels, A. Levin, D. Otzen, D. Klenerman, S. Matthews, S. Linse and M. Andreasen, *et al.*, *Sci. Adv.*, 2022, **8**, eabn6831.
13 S. I. A. Cohen, S. Linse, L. M. Luheshi, E. Hellstrand, D. A. White, L. Rajah, D. E. Otzen, M. Vendruscolo, C. M. Dobson and T. P. J. Knowles, *Proc. Natl. Acad. Sci. U. S. A.*, 2013, **110**, 9758.
14 D. C. Rodriguez Camargo, E. Sileikis, S. Chia, E. Axell, K. Bernfur, R. L. Cataldi, S. I. A. Cohen, G. Meisl, J. Habchi and T. P. J. Knowles, *et al.*, *ACS Chem. Neurosci.*, 2021, **12**, 4406.
15 J. Yang, A. J. Dear, T. C. T. Michaels, C. M. Dobson, T. P. J. Knowles, S. Wu and S. Perrett, *J. Am. Chem. Soc.*, 2018, **140**, 2493pMID: 29357227.
16 M. Andreasen, G. Meisl, J. D. Taylor, T. C. T. Michaels, A. Levin, D. E. Otzen, M. R. Chapman, C. M. Dobson, S. J. Matthews and T. P. J. Knowles, *mBio*, 2019, **10**(1), e02279.
17 P. Arosio, M. Vendruscolo, C. M. Dobson and T. P. J. Knowles, *Trends Pharmacol. Sci.*, 2014, **35**, 127ISSN 0165-6147.
18 T. C. T. Michaels, A. Saric, G. Meisl, G. T. Heller, S. Curk, P. Arosio, S. Linse, C. M. Dobson, M. Vendruscolo and T. P. J. Knowles, *Proc. Natl. Acad. Sci. U. S. A.*, 2020, **117**, 24251.
19 T. C. Michaels, A. J. Dear, S. Cohen, M. Vendruscolo and T. P. J. Knowles, *J. Chem. Phys.*, 2022, **156**, 164904ISSN 0021-9606.
20 G. Salvado, K. Horie, N. R. Barthelemy, J. W. Vogel, A. Pichet Binette, C. D. Chen, A. J. Aschenbrenner, B. A. Gordon, T. L. S. Benzinger and D. M. Holtzman, *et al.*, *Nat. Aging*, 2024, **4**, 694ISSN 2662-8465.
21 A. J. Dear, D. Thacker, S. Wennmalm, L. Ortigosa-Pascual, E. A. Andrzejewska, G. Meisl, S. Linse and T. P. J. Knowles, *ACS Chem. Neurosci.*, 2024, **15**, 2296.
22 G. Brinkmalm, W. Hong, Z. Wang, W. Liu, T. T. O'Malley, X. Sun, M. P. Frosch, D. J. Selkoe, E. Portelius and H. Zetterberg, *et al.*, *Brain*, 2019, **142**, 1441ISSN 0006-8950.
23 M. P. Kummer and M. T. Heneka, *Alzheimer's Res. Ther.*, 2014, **6**, 28ISSN 1758-9193.
24 S. Schilling, A. Pradhan, A. Heesch, A. Helbig, K. Blennow, C. Koch, L. Bertgen, E. H. Koo, G. Brinkmalm and H. Zetterberg, *et al.*, *Acta Neuropathol. Commun.*, 2023, **11**, 87ISSN 2051-5960.

25 A. T. Welzel, J. E. Maggio, G. M. Shankar, D. E. Walker, B. L. Ostaszewski, S. Li, I. Klyubin, M. J. Rowan, P. Seubert and D. M. Walsh, *et al.*, *Biochemistry*, 2014, **53**, 3908ISSN 0006-2960.
26 O. Szczepankiewicz, B. Linse, G. Meisl, E. Thulin, B. Frohm, C. S. Frigerio, M. T. Colvin, A. C. Jacavone, R. G. Griffin and T. Knowles, *et al.*, *J. Am. Chem. Soc.*, 2015, **137**, 14673.
27 J. T. Jarrett, E. P. Berger and P. T. Lansbury, *Biochemistry*, 1993, **32**, 4693.
28 J. Wiltfang, H. Esselmann, P. Cupers, M. Neumann, H. Kretzschmar, M. Beyermann, D. Schleuder, H. Jahn, E. Ruther and J. Kornhuber, *et al.*, *J. Biol. Chem.*, 2001, **276**, 42645ISSN 0021-9258.
29 J. Naslund, A. Schierhorn, U. Hellman, L. Lannfelt, A. D. Roses, L. O. Tjernberg, J. Silberring, S. E. Gandy, B. Winblad and P. Greengard, *Proc. Natl. Acad. Sci. U. S. A.*, 1994, **91**, 8378.
30 R. Cukalevski, X. Yang, G. Meisl, U. Weininger, K. Bernfur, B. Frohm, T. P. J. Knowles and S. Linse, *Chem. Sci.*, 2015, **6**, 4215.
31 G. A. Braun, A. J. Dear, K. Sanagavarapu, H. Zetterberg and S. Linse, *Chem. Sci.*, 2022, **13**, 2423.
32 L. Gu and Z. Guo, *J. Neurochem.*, 2013, **126**, 305.
33 J. Tran, D. Chang, F. Hsu, H. Wang and Z. Guo, *FEBS Lett.*, 2017, **591**, 177.
34 T. Weiffert, G. Meisl, P. Flagmeier, S. De, C. J. R. Dunning, B. Frohm, H. Zetterberg, K. Blennow, E. Portelius and D. Klenerman, *et al.*, *ACS Chem. Neurosci.*, 2019, **10**, 2374.
35 L. Cerofolini, E. Ravera, S. Bologna, T. Wiglenda, A. Boddrich, B. Purfurst, I. Benilova, M. Korsak, G. Gallo and D. Rizzo, *et al.*, *Chem. Commun.*, 2020, **56**, 8830.
36 M. Novo, S. Freire and W. Al-Soufi, *Sci. Rep.*, 2018, **8**, 1783, DOI: **10.1038/s41598-018-19961-3**ISSN 2045-2322.
37 M. Lindberg, E. Axell, E. Sparr and S. Linse, *Biophys. Chem.*, 2024, **307**, 107165ISSN 0301-4622, URL **https://www.sciencedirect.com/science/article/pii/S0301462223002168**.
38 T. C. T. Michaels, C. A. Weber and L. Mahadevan, *Proc. Natl. Acad. Sci. U. S. A.*, 2019, **116**, 14593ISSN 0027-8424.
39 J. R. Espinosa, C. Vega, C. Valeriani, D. Frenkel and E. Sanz, *Soft Matter*, 2019, **15**(47), 9625–9631.
40 F. Grigolato, C. Colombo, R. Ferrari, L. Rezabkova and P. Arosio, *ACS Nano*, 2017, **11**, 11358, DOI: **10.1021/acsnano.7b05895.**pMID: 29045787.
41 F. Grigolato and P. Arosio, *Biophys. Chem.*, 2021, **270**, 106533.
42 Z. Toprakcioglu, A. Kamada, T. C. T. Michaels, M. Xie, J. Krausser, J. Wei, A. Saric, M. Vendruscolo and T. P. J. Knowles, *Proc. Natl. Acad. Sci. U. S. A.*, 2022, **119**, e2109718119.
43 A. J. Dear, G. Meisl, C. G. Taylor, U. C. Palmiero, S. N. Stubbe, Q. Liu, P. Arosio, S. Linse, T. P. J. Knowles and M. Andreasen, *Nanoscale*, 2024, **16**(34), 16172–16182.
44 A. J. Dear, X. Teng, S. R. Ball, J. Lewin, R. I. Horne, D. Clow, A. Stevenson, N. Harper, K. Yahya and X. Yang, *et al.*, *Chem. Sci.*, 2024, **15**, 7229, DOI: **10.1039/D3SC05661A**.
45 G. Meisl, X. Yang, B. Frohm, T. P. J. Knowles and S. Linse, *Sci. Rep.*, 2016, **6**, 18728.
46 K. Brannstrom, T. Islam, A. L. Gharibyan, I. Iakovleva, L. Nilsson, C. C. Lee, L. Sandblad, A. Pamren and A. Olofsson, *J. Mol. Biol.*, 2018, **430**, 1940ISSN 0022-2836.
47 M. Iljina, G. A. Garcia, A. J. Dear, J. Flint, P. Narayan, T. C. T. Michaels, C. M. Dobson, D. Frenkel, T. P. J. Knowles and D. Klenerman, *Sci. Rep.*, 2016, **6**, 28658.
48 M. Baldassarre, C. M. Baronio, L. A. Morozova-Roche and A. Barth, *Chem. Sci.*, 2017, **8**, 8247.
49 D. Thacker, K. Sanagavarapu, B. Frohm, G. Meisl, T. P. J. Knowles and S. Linse, *Proc. Natl. Acad. Sci. U. S. A.*, 2020, **117**, 25272.
50 T. C. T. Michaels, A. Saric, S. Curk, K. Bernfur, P. Arosio, G. Meisl, A. J. Dear, S. I. A. Cohen, C. M. Dobson and M. Vendruscolo, *et al.*, *Nat. Chem.*, 2020, **12**, 445, DOI: **10.1038/s41557-020-0452-1**ISSN 1755-4349.
51 M. Tornquist, R. Cukalevski, U. Weininger, G. Meisl, T. P. J. Knowles, T. Leiding, A. Malmendal, M. Akke and S. Linse, *Proc. Natl. Acad. Sci. U. S. A.*, 2020, **117**, 11265.
52 S. Curk, J. Krausser, G. Meisl, D. Frenkel, S. Linse, T. C. T. Michaels, T. P. J. Knowles and A. Saric, *Proc. Natl. Acad. Sci. U. S. A.*, 2024, **121**, e2220075121.
53 A. J. Dear, G. Meisl, J. Hu, T. P. J. Knowles and S. Linse, *J. Chem. Phys.*, 2025, **163**, 045101, DOI: **10.1063/5.0273677**ISSN 0021-9606.
54 J. Wei, G. Meisl, A. Dear, M. Oosterhuis, R. Melki, C. Emanuelsson, S. Linse and T. P. J. Knowles, *Chem. Sci.*, 2024, **15**, 8430, DOI: **10.1039/D4SC00088A**.
55 A. J. Dear, T. C. T. Michaels, G. Meisl, D. Klenerman, S. Wu, S. Perrett, S. Linse, C. M. Dobson and T. P. J. Knowles, *Proc. Natl. Acad. Sci. U. S. A.*, 2020, **117**, 12087, DOI: **10.1073/pnas.1922267117**ISSN 0027-8424.
56 G. Barenblatt, *Similarity, Self-Similarity, and Intermediate Asymptotics*, Springer, US, 2012, ISBN 9781461585725.
57 C. M. Bender and S. A. Orszag, *Advanced Mathematical Methods for Scientists and Engineers*, Springer, New York, 1999.
58 A. J. Dear and L. Mahadevan, *Proc. R. Soc. A*, 2025, **481**, 20240103URL **https://royalsocietypublishing.org/doi/abs/10.1098/rspa.2024.0103**.
59 N. Ibragimov and V. Kovalev, *Approximate and Renormgroup Symmetries, Nonlinear Physical Science*, Springer, Berlin Heidelberg, 2009, ISBN 9783642002281.
60 D. M. Walsh, E. Thulin, A. M. Minogue, N. Gustavsson, E. Pang, D. B. Teplow and S. Linse, *FEBS J.*, 2009, **276**, 1266.
61 B. Kragelund and K. Skriver, *Intrinsically Disordered Proteins*, Springer, 2020.

